Energy & Environmental Science

Renewable-Integrated Flexible Carbon Capture: A Synergistic Path Forward to Clean Energy Future

Journal:	*Energy & Environmental Science*
Manuscript ID	EE-ART-12-2020-003946.R3
Article Type:	Paper
Date Submitted by the Author:	20-Apr-2021
Complete List of Authors:	Zantye, Manali S.; Texas A&M University Artie Mcferrin Department Of Chemical Engineering Arora, Akhil; Texas A&M University Artie Mcferrin Department Of Chemical Engineering Hasan, M. M. Faruque; Texas A&M University Artie Mcferrin Department Of Chemical Engineering,

Journal Name

ARTICLE TYPE

Cite this: DOI: 00.0000/xxxxxxxxxx

Renewable-Integrated Flexible Carbon Capture: A Synergistic Path Forward to Clean Energy Future†

Manali S. Zantye,[a] Akhil Arora[a] and M. M. Faruque Hasan*[a]

Received Date
Accepted Date

DOI: 00.0000/xxxxxxxxxx

To decarbonize electricity grids, CO_2 capture and renewable wind/solar are two promising pathways. However, the intermittency of these variable renewable sources and the high energy requirement of carbon capture restrict their widespread deployment. These challenges are traditionally addressed independently at the grid-level, leading to conservative costs and limited operational flexibility for both systems. Here, we examine the synergistic integration of renewables and flexible carbon capture with individual fossil power plants. Renewables provide clean energy for carbon capture, while flexible carbon capture acts as a form of energy storage to counter renewable intermittency. To assess whether the benefits obtained from integration outweigh the capital cost under spatiotemporal variability of electricity markets and renewable energy, we develop a mathematical programming-based optimization framework. We decouple the design and operational decisions in a two-stage optimization strategy to efficiently solve the large-scale problem. When applied to a nationwide case study on coal plants across the US, we observe that, for futuristic carbon tax and renewable cost scenarios, it is profitable to invest in solar-assisted carbon capture for nearly one-third of the coal plants. It reduces carbon capture cost by 8.9%, and accommodates solar intermittency while avoiding the capital cost of an equivalent battery, which is 4.4 times the solar farm cost. Furthermore, the levelized cost of electricity will be less than that of new natural gas plants with overall emission reduction between 87.5-91%. The integrated system thereby provides a cost-effective and sustainable measure to reduce CO_2 emissions and improve the operational flexibility of existing fossil-based systems for accelerating the clean energy transition of the global energy sector.

1 Introduction

Coal, petroleum and natural gas contribute to almost two-thirds of the total electricity generation in the US. The CO_2 emissions from these fossil fuels amounted to nearly 93% of the total anthropogenic CO_2 emissions in 2018.[1] The use of CO_2 capture, utilization and storage (CCUS) and the integration of renewable energy sources are two major pathways for reducing the CO_2 emissions from the power sector. For instance, carbon capture alone can reduce power plant emissions by up to 90%.[2–4] The captured CO_2 can be further utilized for enhanced oil recovery (EOR)[5–7] or converted to value-added fuels and chemicals.[8–10] On the other hand, renewables are sustainable with near-zero marginal generation costs.

To achieve a low-carbon grid, however, the challenges in the implementation of these two technologies need to be addressed. Carbon capture is highly energy-intensive, which can reduce the net power output of the plant by 25-40% and drive up power generation costs as much as 70%.[11,12] This limits the widespread deployment of the technology, with currently only two power plants worldwide with fully operational CCUS units.[13] Flexible operation of the capture unit in response to dynamically varying electricity price and demand presents a potential solution to this challenge.[14–17] Flexible carbon capture enables the power plant to reduce CO_2 emissions while maximizing its profit, thereby making CO_2 capture less costly in a dynamic pricing-driven electricity market.

On the other hand, the intermittency and non-dispatchability of variable renewable energy (VRE) sources, especially wind and solar, is a major hurdle in their seamless integration with electricity grids. In the rest of the text, the term renewable energy refers to VRE in the form of wind and solar. Although wind and solar may have some lifecycle CO_2 emissions from their manufacture and construction, they have near-zero direct emissions.[18] Specifically, they have negligible emissions as compared to fossil-based energy sources. Here, we also refer to wind and solar energy

[a] Artie McFerrin Department of Chemical Engineering, Texas A&M University, College Station, TX 77843-3122, USA. Tel: (979) 862-1449; E-mail: hasan@tamu.edu

† Electronic Supplementary Information (ESI) available. See DOI: 00.0000/00000000.

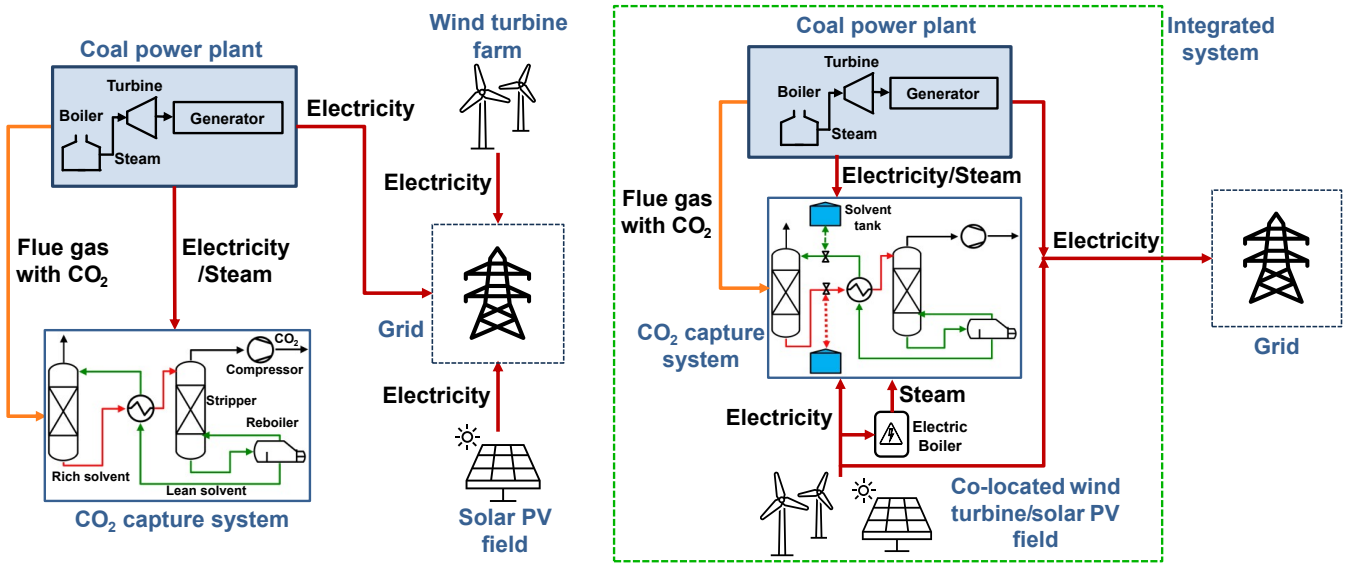

(a) Conventional, non-integrated system configuration.

(b) Integrated system configuration.

Fig. 1 Two paradigms of integrated power generation, CO_2 capture and renewable energy systems. (a) The conventional paradigm only considers the integration of CO_2 capture with coal-based fossil energy generation. The integration of renewable energy with the capture system is typically not considered. The energy required for CO_2 capture is sourced from the power plant alone. There is no interaction between the CO_2 capture system and the renewable energy farms, thereby missing on opportunities for potential synergies. Overall, the cost of integration is high. (b) The proposed paradigm, on the other hand, leverages on the mutually beneficial interaction between the CO_2 capture and renewable energy systems through localized integration with existing power plants. The CO_2 capture system is flexible such that it can dynamically vary the schedule for the energy-intensive solvent regeneration through solvent storage. This allows the solar or wind farm to utilize its surplus energy for CO_2 capture, and reduce the intermittency problem.

sources as clean energy, indicating that they have negligible direct emissions.

To maintain grid reliability under high renewable integration, capital-intensive modifications to grid infrastructure, such as large-scale energy storage and transmission capacities, are required.[19–21] Moreover, due to minimum marginal costs, renewables are the first to be dispatched when they are available, thereby displacing the mid-merit fossil-fueled power plants. These conventional power plants are again forced to rapidly ramp up their output during periods when renewable availability is limited. Such cycling operation of the fossil energy plants to maintain electricity supply and demand balance reduces the overall efficiency and increases operational costs.[22,23]

Traditionally, the integrations of CCUS and renewable energy systems with power plants and electricity grids are attempted independently of each other, resulting in the high cost and limited flexibility for both technologies. Figure 1a illustrates this conventional approach considering the independent integration of carbon capture with coal-based fossil energy generation, and the integration of renewable energy with the electricity grid. CO_2 from the exhaust flue gas of the coal plant is removed in the capture system through solvent-based absorption.[24] The steam energy required to regenerate the CO_2-rich solvent and the electricity required for CO_2 compression are sourced from the power plant alone, thereby significantly reducing its power output. On the other hand, independent grid-level integration of renewable energy requires the cost-intensive storage and transmission measures to mitigate its intermittency.

As policy-makers seek to attain low-carbon grids with increased renewable penetration, it would be difficult to completely phase out fossil energy plants owing to their foothold in the energy mix and their ability to provide reliable back-up power in face of intermittent renewable integration. Albeit its high energy consumption, CCUS provides a sustainable means for the continued use of fossil-based energy. Thus, as we transition to power grids with high renewable penetration, it is important to explore the synergy between these two pathways for decarbonization: renewable energy and carbon capture.

In this work, we hypothesize that the CO_2 emissions from fossil power plants can be effectively reduced by co-investing in a flexible CO_2 capture system and a co-located renewable energy farm, thereby leveraging on the synergies between the two technologies. We investigate the potential of an integrated system including a coal-fired power plant, a CO_2 capture system, a solar PV field and a wind turbine farm. The capture system is flexible in a sense that it can dynamically vary the schedule for the energy-intensive solvent regeneration through solvent storage. The integrated system configuration is depicted through Figure 1b.

Furthermore, we study if investing in the integrated system of CO_2 capture and renewables is more cost-effective as compared to replacing the coal plant with a new natural gas facility to obtain reduced emissions. We demonstrate the framework through both statewide and nationwide case studies on coal plants across the US, and address the following questions through our work:

1. For a coal power plant, is it profitable to invest in a CO_2 capture retrofit and/or a co-located renewable energy farm

to reduce emissions?

2. What is the optimal design of the integrated system considering spatiotemporal variability in electricity prices, solar radiation and wind speed?

3. How does the integrated system cost compare with that of a new natural gas plant?

4. To what extent can renewables reduce the cost of CO_2 capture? Can CO_2 capture effectively counter renewable intermittency?

This article is structured as follows: Section 2 describes the integrated system configuration and lays out the pathway to determine the overall design and operation as a system-wide optimization problem with key decisions. Section 3 presents the optimization-based methodology that allows us to study the large-scale implementation of the integrated system. Sections 4 and 5 illustrate the nationwide and statewide case studies respectively. They present a discussion of the optimization results to address the aforementioned questions. Finally, Section 6 presents a summary of the work and highlights the key findings.

2 Synergistic integration of renewables and carbon capture

The individual challenges of carbon capture and renewables can be possibly addressed if they are operated in tandem. Clean renewable energy can be used to partially meet the energy requirement of carbon capture. Conversely, flexible carbon capture can counter renewable intermittency by dynamic scheduling of solvent regeneration. Such synergy between renewables and carbon capture has been studied in literature mostly at the complete electricity system level, where the impact of carbon capture and renewables to achieve low-carbon, flexible grids has been assessed.[25–29] Among the limited studies at the power plant level, the emphasis is mostly on the integration of a single renewable technology, primarily solar thermal energy. Although the current capital cost of solar thermal systems is more other renewable energy technologies,[30] the advantage of solar thermal systems lies in the conversion of solar energy to steam, which can be directly used for solvent regeneration in the capture system for CCUS.

Parvareh et al.[31] presented a comprehensive review on the different configurations of integrating solar thermal energy with coal plants. Cohen and Rochelle[32] performed preliminary feasibility studies on using solar thermal energy for the complete and partial compensation of the CO_2 reboiler heat duty. Mokhtar et al.[33] conducted a techno-economic assessment of integration for coal plants in Australia using actual weather and electricity market data. The feasibility analysis by Li et al.[34] showed that the local climatic conditions play a crucial role in the economic viability of solar integration. Qadir et al.[35] determined the optimal operation of a solar-assisted coal plant with CO_2 capture through dynamic modeling and optimization. They inferred that the integration is viable in regions where solar energy availability coincides with high electricity prices and load demand. Zhao et al.[36] compared two configurations of integrating mid-temperature solar-generated steam in a coal plant with CO_2 capture. They found that the integration increases overall power output from the plant by nearly 17% as compared to a non-hybridized system.

Apart from solar thermal energy, the second most common technology considered for integration is wind energy. Kang et al.[37] studied a modular system comprising of a coal plant with CO_2 capture integrated with a natural gas combustion turbine and wind energy. They compared the performance of a heuristic procedure and a local optimization algorithm to maximize the profit from the integrated system. Bandyopadhyay and Patiño-Echeverri[38] determined the optimal design and operation of a coal-wind hybrid system. Phadke et al.[39] studied a coal gasification unit with CCS integrated with wind energy. They concluded that the hybrid system has a lower levelized cost of electricity (LCOE), or the net present cost incurred per unit of electricity generated, compared to an independent coal/wind system owing to the avoided cost of building additional transmission lines for wind integration.

Additionally, there are few studies on integrating biomass as well as solar photovoltaics (PV). Carapellucci et al.[40] studied the integration of an auxiliary biomass boiler and a concentrated solar power (solar thermal) technology with a coal power plant with CO_2 capture. Similarly, Khorshidi et al.[41] investigated the use of an auxiliary biomass-based unit to provide both the heat and electricity requirements of the CO_2 capture system. They performed a techno-economic analysis and provided estimates of CO_2 and biomass prices to make the integration economically attractive. Gouse et al.[42] considered several integration options of PV systems with integrated gasification combined cycle (IGCC) power plants to reduce emissions. Most of these studies focus on using renewable integration to supply the steam energy required for the solvent regeneration reboiler of the CO_2 capture system. The energy consumption of auxiliary units, such as pumps, blowers and CO_2 compressors, amounts to nearly 50% of the equivalent work requirement of the reboiler,[43] but is often overlooked. This energy penalty is assumed to be parasitically drawn from the power plant.

Till now, the predominant focus has been on the feasibility aspect of integration, often ignoring the optimization of both the design and operational decisions. The high upfront cost of renewable technologies and their intermittent availability has a direct impact on the economic viability of the integration.[33] Thus, it is important to determine both the optimal investment and operating decisions of the integrated system.

There are several benefits to considering the localized integration, as shown in Figure 1b, as compared to the conventional grid-level analysis. Firstly, renewable integration with the grid is facilitated without the costly grid-level modifications. Secondly, to accommodate the variable renewable energy, the flexible carbon capture operation also improves the operational flexibility of individual power plants without frequent cycling operation. In face of high renewable availability, carbon capture can reduce power output from the plant thereby keeping it online for longer durations. Similarly, the capture operation can be turned down to meet peak power requirements at times when renewables are not readily available. Thirdly, the installation of additional transmission capacities for renewable integration is eliminated. In the

integrated system, the renewable energy farm delivers electricity to the grid using the transmission lines of the power plant and the transmission capacity generated from flexible carbon capture operation.

We consider a combination of renewable technologies for potential integration: both solar PV and onshore wind systems, as opposed to the single technology analysis which is commonly done. This counters the limitations of the latter, such as the requirement of a high-efficiency solar field with thermal storage to meet the capture energy penalty through solar integration alone. We hypothesize that the consideration of a mix of renewable technologies can distribute the onus of capture penalty compensation over the individual technologies depending on their availability. This can potentially avoid the reliance on a single highly efficient technology. Additionally, to maximize the utilization of clean renewable energy in compensating the carbon capture energy penalty, we consider its use to provide the electricity required in the capture system's auxiliary components along with the provision of steam for solvent regeneration.

To illustrate the interaction among the various system components, the integrated system of the coal-based unit, renewables and carbon capture is concisely represented using a superstructure shown by Figure 2. The energy sources include the coal power plant, and the renewable energy technologies i.e. wind and solar PV. Exhaust flue gas generated from the coal plant with a typical CO_2 concentration of 15 vol.% is directed to the capture system for solvent-based CO_2 separation and removal. The extracted CO_2 is compressed and sent to downstream units for further utilization. The energy sinks in the superstructure consist of the electricity grid and the various stages of the capture system, such as the CO_2 absorption, desorption (solvent regeneration), and compression sections. Among the capture system components, the CO_2 desorption step is the most energy-intensive with energy requirement in the form of steam.

The three energy sources generate energy in the form of electricity. The generated electricity is delivered to the grid and/or used to meet the electricity requirement of CO_2 capture, i.e. in the CO_2 absorption and compression systems. Power requirement in the absorption section stems from auxiliary units such as pumps to circulate the solvent. The steam required for CO_2 desorption from the solvent is sourced by directing a portion of the steam from the intermediate and low-pressure steam turbines of the coal power plant. To maximize the use of renewable energy for CO_2 capture, we consider the use of an electric boiler to produce steam from renewable-generated electricity. This steam is used in the CO_2 desorption step, along with steam extracted from the coal power plant.

Along with meeting the energy requirement of CO_2 capture, renewables provide a clean energy source for the system to meet the grid electricity demand and generate revenue. On the other hand, flexible CO_2 capture helps in handling the intermittency of renewables by acting in the form of an energy storage system. During periods of low electricity price or grid demand and excess renewable availability, the CO_2 capture operation is ramped up and the surplus energy is utilized for capture. Conversely, the capture operation is turned down during peak grid demand periods and low renewable availability to increase the energy delivered to the grid.

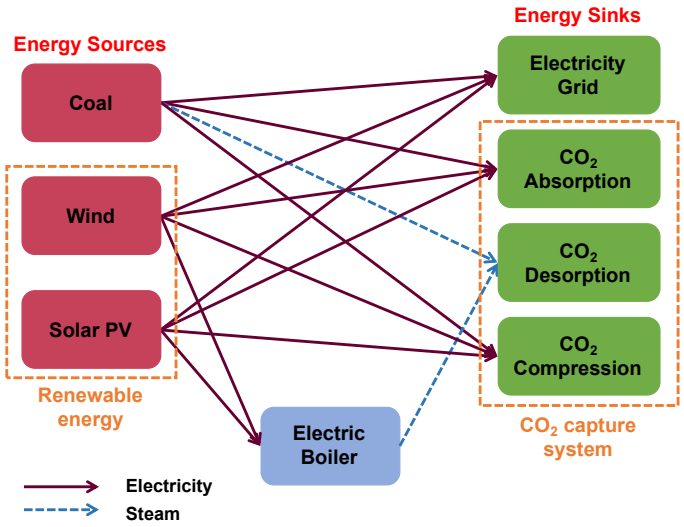

Fig. 2 Plausible ways of integrating energy sources and sinks. A coal power plant, for example, can meet the energy demand of the electricity grid. It can also supply the required energy for CO_2 capture. The wind/solar PV can do the same. Furthermore, the electricity generated by the wind and solar is converted to steam using an electric boiler, for use in solvent regeneration. The challenge is, however, to obtain the optimal connectivity and network configuration that will maximize the energy economics of the system.

The economics of this configuration is impacted by the high capital cost of the system components and the spatiotemporal variability of electricity price and renewable availability. To incorporate the cost-emission trade-offs in optimal decision making, we propose a mathematical programming-based optimization approach to determine the conditions under which the benefits accrued by a coal power plant through a carbon capture retrofit or a co-located renewable farm installation outweigh the capital investment of these systems.

We define the problem statement as follows: for given time-varying electricity price, solar irradiation intensity and wind speed profiles, determine the optimal design and operational decisions of integration with an existing coal power plant which maximizes its net present value (NPV). NPV signifies the present value of the investment based on projected costs and earnings of the system. The design decisions include: (i) retrofit of the coal plant with a CO_2 capture system, (ii) installation of co-located wind/solar PV fields and their nominal capacities, and (iii) investment in an electric boiler and its capacity. The dynamic operational decisions comprise of: (i) the extent of flexible capture system operation i.e. the rates of CO_2 absorption, desorption and compression, and (ii) the power flow among the various system components.

3 Methodology

The optimization objective is to simultaneously determine the long-term design and the hourly operational decisions under given, deterministic profiles of electricity price, solar radiation and wind speed. However, developing a unified approach to

determining the optimal integration configuration in our system is computationally non-trivial due to the multi-scale variability exhibited by intermittent renewable energy as well as electricity markets. Specifically, electricity price and renewable energy availability display high-frequency and low-frequency temporal variability depending on the time of the day and season. Also, there is significant spatial variation of these parameters based on geographic location.

To solve this multi-scale problem with design decisions spanning several years and operating decisions focusing on shorter time periods, we employ a two-stage solution strategy. The two-stage framework decouples the complicating design decisions from the hourly operating decisions and enables us to solve the large-scale optimization problem in a computationally tractable manner. To the best of our knowledge, such a framework has not been applied previously in this particular application of integrating renewable energy and CO_2 capture with coal plants. The optimization formulation and the two-stage solution strategy are described below.

3.1 Integrated system model formulation

The assumptions which prelude the model development are as follows:

- Each year is identical in terms of electricity price, solar radiation and wind speed. The system operation does not vary from year to year, resulting in the same cash flow.
- Considering an existing coal power plant, its nameplate capacity and base-case emission intensity i.e. emission intensity of the stand-alone power plant (ton CO_2/MWh), are fixed.
- Complete shutdown of the power plant is not considered. The power plant always operates with output between its minimum turndown and nominal capacity.
- The specific solvent consumption for CO_2 absorption (kg/kg CO_2) is assumed to be a constant. Additionally, the specific energy penalty (MWh/kg CO_2) of the capture system absorption, desorption and compression sections is a constant. There is no loss of solvent in the capture system.
- The size of the capture system scales linearly with respect to a reference power plant case with given nameplate capacity and emission intensity. Similarly, the maximum rich and lean solvent flowrates are determined as a linear function of the reference case solvent flowrate. A fixed maximum storage duration is assumed.
- The maximum power output of the system is the same as the coal plant nameplate capacity, avoiding the installation of additional power transmission lines for integration. The system is contractually obligated to produce a pre-determined fraction of this maximum capacity at each hour which is sold to the grid at a fixed price. Power output in excess of this is then sold in the electricity spot market subject to variable price profiles.
- There exist policy measures to provide economic incentive for the reduction of carbon emissions from the power plant. These measures include both a tax on CO_2 emissions as well as a selling price on the utilized CO_2. The selling price of CO_2 can be in the form of the price on carbon credits earned through the utilization of the captured CO_2 for end-uses such as EOR or conversion to value-added fuels and chemicals (methanol, methane, dimethyl ether, gasoline, etc.). Such CO_2 utilization may not be restricted to EOR only. The CO_2 can also be further purified to increase its commercial value for utilization in high purity applications, for instance in the food and beverage industry.[44] This utilization route represented the second most common end-use of captured CO_2 in the US in 2019.[45,46] The costs for CO_2 conversion and purification downstream are not included in the current work.

Temporal variability in electricity price, wind speed and solar radiation is represented through deterministic scenarios, where $\omega \in \Omega = \{1,2,...,NS\}$ represents a scenario, and Ω denotes the set of scenarios in a year with hourly resolution. Furthermore, p_ω denotes the deterministic frequency of scenario occurence, which follows:

$$\sum_{\omega \in \Omega} p_\omega = 1. \tag{1}$$

For ease of comparison between the availability of the two resources, the actual renewable power output determined by the wind speed or solar irradiation is normalized with the maximum possible output using the capacity factor. Specifically, capacity factor of wind turbines $cf_{w,\omega}$ is calculated as a dimensionless cubic function of wind speed $v_{w,\omega}$ through the given power curve:[47]

$$\begin{aligned}
cf_{w,\omega} &= 0, && v_{w,\omega} < v_w^{ci}, \\
cf_{w,\omega} &= \frac{{v_{w,\omega}}^3 - {v_w^{ci}}^3}{{v_w^r}^3 - {v_w^{ci}}^3}, && v_w^{ci} \le v_{w,\omega} \le v_w^r, \\
cf_{w,\omega} &= 1, && v_w^r < v_{w,\omega} \le v_w^{co}, \\
cf_{w,\omega} &= 0, && v_{w,\omega} > v_w^{co},
\end{aligned} \tag{2}$$

where, $v_w^{ci}, v_w^r, v_w^{co}$ denote the wind turbine cut-in, rated and cut-off wind speeds respectively. The effect of turbine hub height on capacity factor is not considered in Eq. 2. Similarly, Eq. 3 represents the capacity factor of solar PV arrays as a fraction of the actual solar irradiation at scenario ω, H_ω, to the reference irradiation of the solar panel, H^{ref}.[48] $\eta^{arr}, \eta^{dc/ac}$ and η^{wir} signify the PV array, DC-to-AC conversion and wiring efficiency respectively. Here, we do not consider the effect of ambient temperature on efficiency.

$$cf_{sp,\omega} = \frac{H_\omega}{H^{ref}} \eta^{arr} \eta^{dc/ac} \eta^{wir} \tag{3}$$

The various model attributes along with the overall NPV maximization model are described below.

3.1.1 Sets, indices and variables.

We define $\mathscr{T}$ and $\mathscr{M}$ as two master sets and consider other sets to be subsets of these. $\mathscr{T}$ represents the set of time steps

in the scheduling horizon and $\mathscr{M}$ includes the system components shown in the superstructure of Figure 2. The index $t \in \mathscr{T} = \{1,2,...,NT\}$ denotes a time step, while $m,m' \in \mathscr{M} = \{cl,w,sp,g,a,d,c,b\}$ denotes a superstructure block. Here, the coal, wind and solar energy sources are represented as cl,w and sp respectively. The electric boiler is denoted by b and the energy sinks comprising the grid, CO_2 capture absorption, desorption and compression sections are represented as g,a,d and c respectively.

The subsets of the master set $\mathscr{M}$ include the set of energy sources: $sor_m = \{cl,w,sp\}$, set of energy sinks: $sks_m = \{g,a,d,c\}$, renewable sources set: $ren_m = \{w,sp\}$ and the set of blocks representing the CO_2 capture system: $capt_m = \{a,d,c\}$. Additionally, to represent the energy flows between the blocks, we define subsets I_m and J_m. I_m denotes the set of blocks from which there is energy input to block $m \in \mathscr{M}$, where $I_b = \{w,sp\}, I_g = \{cl,w,sp\}, I_a = \{cl,w,sp\}, I_d = \{cl,b\}, I_c = \{cl,w,sp\}$. Similarly, J_m signifies the set of blocks to which there is energy output from block $m \in \mathscr{M}$, where $J_{cl} = \{g,a,d,c\}, J_w = \{g,a,b,c\}, J_b = \{d\}, J_{sp} = \{g,a,b,c\}$.

The design decision variables include the binary variable for carbon capture retrofit b^{ret}, installed capacity of the renewable energy technologies sz_w, sz_{sp}, and electric boiler capacity sz_b. The scenario-dependent operational decision variables comprise of the power flow from block m to m', $P^{flow}_{m,m',\omega}$, and the capture system flexible operation $r_{a,\omega}, r_{d,\omega}$. Here, $r_{a,\omega}$ and $r_{d,\omega}$ denote the rates of CO_2 absorption and desorption respectively. These can be further represented as the ratio of the amount of CO_2 absorbed, desorbed or compressed in scenario ω to the amount of CO_2 processed for inflexible operation at 100% capture load.

For instance, a power plant with nameplate capacity p^{max}_{cl} (MW) and base-case CO_2 emission intensity of E_{cl} (ton MWh^{-1}) will have CO_2 emissions equal to $p^{max}_{cl} E_{cl}$ (ton h^{-1}) if operated at maximum load. If this plant has a capture system installed with the absorber, desorber and compressor kept at maximum load, the amount of CO_2 absorbed from the flue gas would be given by $\gamma_a\, p^{max}_{cl} E_{cl}$ (ton h^{-1}), where γ_a is the CO_2 removal rate of the absorber (90%). As there is no storage of solvent in the inflexible case, the amount of CO_2 desorbed and compressed at any time scenario would also be equal to $\gamma_a\, p^{max}_{cl} E_{cl}$. The variables $r_{a,\omega}$ and $r_{d,\omega}$ then define the amount of CO_2 absorption and desorption taking place for the flexible case with solvent storage as compared to the inflexible case of maximum capture rate. As the capture system may not absorb 90% CO_2 from the power plant flue gas during flexible operation, the amount of CO_2 absorbed at scenario ω is $r_{a,\omega}\, \gamma_a\, p^{max}_{cl} E_{cl}$. Here, $r_{a,\omega}$ denotes the fractional absorption rate that varies between 0 and 1. Similarly, due to the solvent storage, the amount of CO_2 desorbed at scenario ω is given by $r_{d,\omega}\, \gamma_a\, p^{max}_{cl} E_{cl}$.

The remaining variables in the model are given in Table 1.

Table 1 Mathematical model variables

Variable	Description	Unit
NPV	Net present value	\$
CC^{tot}	Total capital cost	\$
PF^{net}	Net profit	\$ yr^{-1}
PF^{gro}	Gross profit	\$ yr^{-1}
Rev_ω	Revenue for scenario ω	\$ h^{-1}
$Cost_\omega$	Operating cost for scenario ω	\$ h^{-1}
$P^{in}_{m,\omega}$	Power input to block m for scenario ω	MW
$P^{out}_{m,\omega}$	Power output from block m for scenario ω	MW
M^{capt}_ω	Compressed CO_2 for scenario ω	ton h^{-1}
M^{em}_ω	Net CO_2 emissions for scenario ω	ton h^{-1}
M^{flue}_ω	CO_2 in power plant flue gas for scenario ω	ton h^{-1}
$RC_{cl,\omega}$	Ramping costs of coal plant for scenario ω	\$
V^{rich}_ω	Volume of rich solvent tank for scenario ω	m^3
V^{lean}_ω	Volume of lean solvent tank for scenario ω	m^3

3.1.2 NPV maximization model.

The optimization formulation maximizing the NPV of the integrated system is given below. The overall model is a mixed-integer linear programming (MILP) problem.

$$\text{M1: max } NPV = -CC^{tot} + \frac{CC^{tot}}{t^{dp}}\, r^{tax}\left(\frac{1}{r^{disc}} - \frac{1}{r^{disc}\,(1+r^{disc})^{t^{dp}}}\right) + PF^{net}\left(\frac{1}{r^{disc}} - \frac{1}{r^{disc}\,(1+r^{disc})^{t^{lf}}}\right) \tag{4a}$$

$$\text{s.t. } CC^{tot} = \sum_{m\in ren} CO_m\, sz_m + CO_b\, sz_b + \left(CO^{capt}\, p^{max}_{cl}\, \frac{E_{cl}}{E^{ref}_{cl}}\frac{I^{17}}{I^{02}} + N^{tank} CO^{tank} sz^{tank}\right) b^{ret}, \tag{4b}$$

$$PF^{net} = (1 - r^{tax})\, PF^{gro}, \tag{4c}$$

$$PF^{gro} = \sum_{\omega\in\Omega} t_\omega\, (Rev_\omega - Cost_\omega), \tag{4d}$$

$$Rev_\omega = p^l \pi^l + (P^{in}_{g,\omega} - p^l)\pi^s_\omega + M^{capt}_\omega \pi^{csp},\ \forall \omega \in \Omega, \tag{4e}$$

$$Cost_\omega = P^{out}_{cl,\omega}\, C^{gen}_{cl} + M^{em}_\omega C^{em} + M^{capt}_\omega C^{ts} + \frac{RC_{cl,\omega}}{t_\omega},\ \forall \omega \in \Omega, \tag{4f}$$

$$RC_{cl,\omega} \geq C^{ramp}\left(P^{out}_{cl,\omega+1} - P^{out}_{cl,\omega}\right),\ \forall \omega \in \Omega \setminus \{NS\}, \tag{4g}$$

$$RC_{cl,\omega} \geq C^{ramp}\left(P^{out}_{cl,\omega} - P^{out}_{cl,\omega+1}\right),\ \forall \omega \in \Omega \setminus \{NS\}, \tag{4h}$$

$$RC_{cl,\omega=NS} = 0, \tag{4i}$$

$$P^{in}_{m,\omega} = \sum_{m'\in I_m} P^{flow}_{m',m,\omega},\ \forall m \in \mathscr{M},\ \forall \omega \in \Omega, \tag{4j}$$

$$P^{out}_{m,\omega} = \sum_{m'\in J_m} P^{flow}_{m,m',\omega},\ \forall m \in \mathscr{M},\ \forall \omega \in \Omega, \tag{4k}$$

$$\sum_{m\in sor} P^{out}_{m,\omega} = \sum_{m\in sks} P^{in}_{m,\omega} + (P^{in}_{b,\omega} - P^{out}_{b,\omega}),\ \forall \omega \in \Omega, \tag{4l}$$

$$lf_{cl}^{min}\ p_{cl}^{max} \leq P_{cl,\omega}^{out} \leq p_{cl}^{max},\ \forall \omega \in \Omega, \tag{4m}$$

$$-\Delta p_{cl}^{max}\ t_\omega \leq P_{cl,\omega+1}^{out} - P_{cl,\omega}^{out} \leq \Delta p_{cl}^{max}\ t_\omega,\ \forall \omega \in \Omega \setminus \{NS\}, \tag{4n}$$

$$P_{m,\omega}^{out} = cf_{m,\omega}\ sz_m,\ \forall m \in ren,\ \forall \omega \in \Omega, \tag{4o}$$

$$p^l \leq P_{g,\omega}^{in} \leq p_{cl}^{max},\ \forall \omega \in \Omega, \tag{4p}$$

$$M_\omega^{flue} = P_{cl,\omega}^{out}\ E_{cl},\ \forall \omega \in \Omega, \tag{4q}$$

$$M_\omega^{capt} = r_{c,\omega}\ p_{cl}^{max}\ E_{cl}\ \gamma_a,\ \forall \omega \in \Omega, \tag{4r}$$

$$M_\omega^{em} = M_\omega^{flue} - r_{a,\omega}\ p_{cl}^{max}\ E_{cl}\ \gamma_a,\ \forall \omega \in \Omega, \tag{4s}$$

$$r_{d,\omega} = r_{c,\omega},\ \forall \omega \in \Omega, \tag{4t}$$

$$0 \leq r_{a,\omega} \leq b^{ret}\ r_a^{max},\ \forall \omega \in \Omega, \tag{4u}$$

$$0 \leq r_{d,\omega} \leq b^{ret}\ r_d^{max},\ \forall \omega \in \Omega, \tag{4v}$$

$$-\Delta r_a^{max}\ t_\omega \leq r_{a,\omega+1} - r_{a,\omega} \leq \Delta r_a^{max}\ t_\omega,\ \forall \omega \in \Omega \setminus \{NS\}, \tag{4w}$$

$$-\Delta r_d^{max}\ t_\omega \leq r_{d,\omega+1} - r_{d,\omega} \leq \Delta r_d^{max}\ t_\omega,\ \forall \omega \in \Omega \setminus \{NS\}, \tag{4x}$$

$$P_{a,\omega}^{in} = \mu_a\ p_{cl}^0\ r_{a,\omega},\ \forall \omega \in \Omega, \tag{4y}$$

$$P_{d,\omega}^{in} = \mu_d\ p_{cl}^0\ r_{d,\omega},\ \forall \omega \in \Omega, \tag{4z}$$

$$P_{c,\omega}^{in} = \mu_c\ p_{cl}^0\ r_{c,\omega},\ \forall \omega \in \Omega, \tag{4aa}$$

$$V_{\omega+1}^{rich} = V_\omega^{rich} + S^{max}\left(r_{a,\omega} - r_{d,\omega}\right)t_\omega,\ \forall \omega \in \Omega \setminus \{NS\}, \tag{4ab}$$

$$V_{\omega+1}^{lean} = V_\omega^{lean} + S^{max}\left(r_{d,\omega} - r_{a,\omega}\right)t_\omega,\ \forall \omega \in \Omega \setminus \{NS\}, \tag{4ac}$$

$$V_1^{rich} = V_0^{rich} + S^{max}\left(r_{a,1} - r_{d,1}\right)t_1, \tag{4ad}$$

$$V_1^{lean} = V_0^{lean} + S^{max}\left(r_{a,1} - r_{d,1}\right)t_1, \tag{4ae}$$

$$V_0^{rich} = V_{NS}^{rich}, \tag{4af}$$

$$V_0^{lean} = V_{NS}^{lean}, \tag{4ag}$$

$$0 \leq V_\omega^{rich} \leq sz^{tank},\ \forall \omega \in \Omega, \tag{4ah}$$

$$0 \leq V_\omega^{lean} \leq sz^{tank},\ \forall \omega \in \Omega, \tag{4ai}$$

$$0 \leq sz_b \leq \sum_{m \in ren} sz_m, \tag{4aj}$$

$$0 \leq P_{b,\omega}^{in} \leq sz_b,\ \forall \omega \in \Omega, \tag{4ak}$$

$$P_{b,\omega}^{out} = P_{b,\omega}^{in}\ \eta^b \eta^{te},\ \forall \omega \in \Omega, \tag{4al}$$

$$b^{ret} \in \{0,1\},\ sz_w \in \mathbb{R}^+,\ sz_{sp} \in \mathbb{R}^+,\ sz_b \in \mathbb{R}^+,$$

$$P_{m,m',\omega}^{flow} \in \mathbb{R}^+,\ r_{a,\omega} \in \mathbb{R}^+,\ r_{d,\omega} \in \mathbb{R}^+,\ \forall \omega \in \Omega.$$

The objective function of net present value can be expressed as the difference between the system's future cash flows discounted for the time value of money and the current investment cost incurred. The first term in Eq. 4a denotes the total capital cost of the system. The system earns tax savings on this initial investment every year owing to depreciation. The present value of this tax saving is expressed using the second term assuming straight line depreciation. The third term represents the present value of system earnings over the project lifetime or the discounted net annual profit. Owing to the assumption of each year to be identical, the cash flow is the same per year, PF^{net}.

Eq. 4b denotes the total capital cost of the integrated system as the sum of individual costs of the renewable energy farm, electric boiler and the CO_2 capture system including solvent storage tanks. Furthermore, the net profit can be expressed as the gross profit earned per year less any applicable taxes, given by Eq. 4c. Eq. 4d represents the yearly gross profit as the sum of cash flow over all scenarios in a year, determined by the difference between the total revenue earned and cost incurred. A weightage is assigned to the earnings in a particular scenario ω depending on the length of time, t_ω, of the scenario occurrence in a year. This weightage is derived from the scenario frequency p_ω and number of operating hours h^{op} such that

$$t_\omega = p_\omega\ h^{op},\ \ \forall \omega \in \Omega. \tag{5}$$

The various financial parameters in Eqs. 4a - 4d are given in Table S1 of the ESI.† Eq. 4e depicts the scenario-based system revenue as the sum of individual components. The three terms in Eq. 4e represent the revenue earned by the system from long-term contracts, in the spot market and through the sale of the captured CO_2, respectively.

Furthermore, the various operating cost components, given in Eq. 4f include: power generation costs for the coal power plant including fuel costs and variable operating and maintenance (O&M) costs, costs associated with CO_2 emissions owing to environmental regulations, costs of storing and transporting the captured CO_2 to end-use sites (T&S cost) and finally, ramping costs associated with flexible power plant operation. Since we consider the coal power plant to be an existing facility, the capital costs and fixed costs associated with its design are not considered in the cost equations. Since flexible operation of the coal power plant designed typically for base-load has a detrimental effect on critical components owing to the build-up of thermal and mechanical stresses, the resulting increase in operating and maintenance cost is accounted for through Eqs. 4g-4i. The revenue and cost parameters used in the model are given in Table S3 of the ESI.†

Eqs. 4j-4l represent the energy balance equations for the system. In Eq. 4l, we are also accounting for the loss of energy in the electric boiler due to its efficiency of steam generation. Bounds on power output from the coal power plant are given in Eq. 4m. The maximum power output is given by the nameplate capacity and

the turndown limit is determined by the minimum load factor. Eq. 4n depicts ramping constraints on the power plant output. Power output from renewable energy sources is determined by Eq. 4o as a product of the capacity factor and installed capacity. Furthermore, Eq. 4p represents the bounds on the total power delivered by the system to the grid, with the minimum power output to be that pre-determined by the contractual agreement and the maximum output equal to the coal plant nameplate capacity.

Eqs. 4q-4ai depict the constraints on the CO_2 capture system and are derived from our previous work on flexible CO_2 capture.[14] A short summary is presented here; interested readers can refer to the aforementioned work for further information. The capture model is based on a chemical absorption-based CO_2 separation process that uses 30% by weight aqueous monoethanolamine (MEA) solution as the solvent. MEA-absorption is a widely considered technology that is suitable for capturing CO_2 from power plants.[2] The typical operating conditions for the MEA-based process are as follows: The flue gas consists of 12 vol% CO_2, 10 vol% H_2O, 73 vol% N_2 and 4 vol% O_2. The absorber pressure is 1 atm with a temperature of 40 °C. The stripper bottom pressure is 1.7 atm with a temperature of 120 °C. The purity of recovered CO_2 is 99 vol%. The CO_2 is compressed to an end pressure of 13.7 MPa for transportation. To enable a high-level nationwide analysis for integration, we use mathematical models from literature to represent the dynamic operation of the CO_2 capture process. These models, based on the work of Chen et al.,[49] use linear functions to relate the partial load of absorption and desorption columns to their energy consumption. The linearization facilitates computational tractability without significant loss of accuracy in the large-scale optimization problem. In addition, a detailed discussion on the specifics of the capture system considered, potential improvements and comparison with other capture technologies are included in Section S2 of the ESI.†

The amount of CO_2 captured and resulting power consumption in the flexible operation is expressed in comparison to the inflexible capture case using relative rates $r_{a,\omega}, r_{d,\omega}, r_{c,\omega}$. To maintain consistency, the thermal energy consumption of the stripper is represented in terms of equivalent electricity consumed in Eq. 4z. We assume both solvent tanks to be initially half-filled. To ensure that each year is identical, cyclical conditions are imposed on the system through Eqs. 4af-4ag which indicate the initial solvent storage volume to be the same as that at the end of a year.

Eqs. 4aj - 4al denote the design and operational constraints for the electric boiler. The upper bound on boiler size is determined by the installed capacity of renewables as given by Eq. 4aj. This also indicates that the boiler capacity is zero (no boiler selected) when there is no renewable integration. Electric power output corresponding to the steam energy produced is calculated assuming a constant thermal energy to electricity conversion factor η^{te} in Eq. 4al. This represents the equivalent power production if the generated LP steam were to be used in the coal power plant turbine to produce electricity. The various system design and operational parameters are given in Table S2 of the ESI.†

3.2 Solution strategy

The major challenge in optimization lies in striking an appropriate balance between computational tractability of the model and solution accuracy. Although hourly discretized time-varying profiles over a year sufficiently capture the seasonal and daily variation of electricity price and renewable availability, it tremendously increases the computational complexity in simultaneously solving for system design and operation. Time-aggregation or temporal clustering is a popular method to handle the complexity, wherein time periods with similar parameter profiles are grouped together and reduced number of scenarios adequately representing the parameter variability are obtained.[50–55]

The overall problem is then recast to two stages. In the first stage, the reduced scenarios are used to solve for the optimal system design. The second stage then optimizes the scenario-based system operation for a given design. The overall solution strategy is discussed below.

3.2.1 General formulation.

To implement the two-stage solution strategy decoupling the design and operational decisions, we represent the overall NPV maximization model M1 in a general form as follows:

$$\text{M0}: \max_{\mathbf{x},\, \mathbf{y}_\omega} \; f_d(\mathbf{x}) + \sum_{\omega\in\Omega} p_\omega f_o(\mathbf{x}, \mathbf{y}_\omega, \mathbf{k}_\omega) \tag{6a}$$

$$\text{s.t. } \mathbf{g}^{(\text{d})}(\mathbf{x}) \le 0, \tag{6b}$$

$$\mathbf{h}^{(\text{d})}(\mathbf{x}) = 0, \tag{6c}$$

$$\mathbf{g}^{(\text{o})}(\mathbf{x}, \mathbf{y}_\omega, \mathbf{k}_\omega) \le 0, \; \forall \omega \in \Omega, \tag{6d}$$

$$\mathbf{h}^{(\text{o})}(\mathbf{x}, \mathbf{y}_\omega, \mathbf{k}_\omega) = 0, \; \forall \omega \in \Omega, \tag{6e}$$

$$\mathbf{s}^{(\text{o})}(\mathbf{x}, \mathbf{y}_\omega, \mathbf{y}_{\omega+1}) = 0, \; \forall \omega \in \Omega. \tag{6f}$$

Here, $\mathbf{x}$ is a vector representing the design decisions, while the vector $\mathbf{y}_\omega$ encapsulates the scenario-dependent operational decisions. The set $\mathbf{k}_\omega$ represents the external parameters associated with scenario ω. The objective function consists of two components: (i) f_d, which depends on design decisions alone, and (ii) f_o determined through both the design and operational decisions. On comparison with the overall formulation M1, we can represent the two components as follows:

$$f_d(\mathbf{x}) = -CC^{tot} + \frac{CC^{tot}}{t^{dp}}\, r^{tax} \left(\frac{1}{r^{disc}} - \frac{1}{r^{disc}\,(1+r^{disc})^{t^{dp}}} \right), \tag{7a}$$

$$f_o(\mathbf{x}, \mathbf{y}_\omega, \mathbf{k}_\omega) = (1 - r^{tax}) \left(\frac{1}{r^{disc}} - \frac{1}{r^{disc}\,(1+r^{disc})^{t^{lf}}} \right) \times (Rev_\omega - Cost_\omega). \tag{7b}$$

$\mathbf{g}^{(\text{d})}(\mathbf{x})$ and $\mathbf{h}^{(\text{d})}(\mathbf{x})$ are the inequality and equality constraints on system design, represented by Eqs. 4aj and 4b respectively. $\mathbf{g}^{(\text{o})}(\mathbf{x}, \mathbf{y}_\omega, \mathbf{k}_\omega)$ and $\mathbf{h}^{(\text{o})}(\mathbf{x}, \mathbf{y}_\omega, \mathbf{k}_\omega)$ denote the inequality and equality constraints on system operation. $\mathbf{g}^{(\text{o})}(\mathbf{x}, \mathbf{y}_\omega, \mathbf{k}_\omega)$ is represented by Eqs. 4m, 4p, 4u -4v, 4ah-4ai, 4ak of model M1. On the other

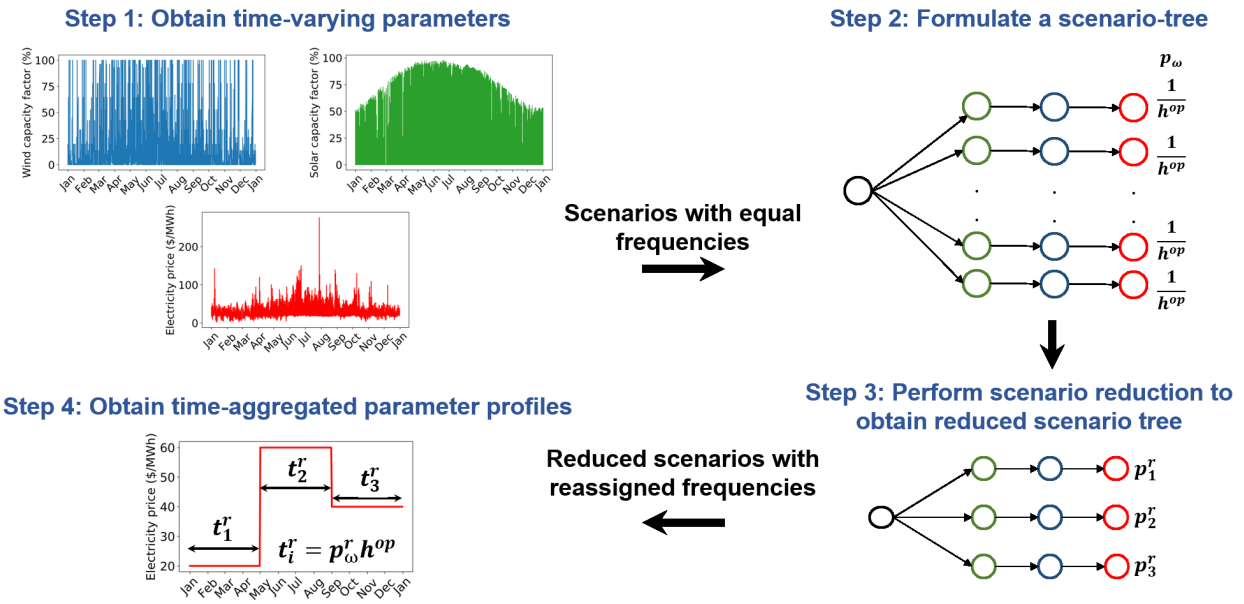

Fig. 3 Time-aggregation process of parameter profiles via scenario reduction through SCENRED.[56] Starting from hourly discretized data for a representative year, we first obtain the time-varying input parameters. We then formulate the scenario tree and assign the scenario frequencies, assuming that each branch has an equal frequency. This allows us to directly employ the SCENRED[56] package in GAMS[57] to perform scenario reduction and obtain the reduced scenario tree along with the re-assigned frequencies. Finally, we transform the scenario tree into time-aggregated parameter profiles. These profiles are used to determine the optimal system design.

hand, the set of equality constraints $\mathbf{h}^{(o)}(\mathbf{x},\mathbf{y}_\omega,\mathbf{k}_\omega)$ is denoted by Eqs. 4c -4f, 4j-4l, 4o, 4q-4t, 4y-4aa, 4al. $\mathbf{s}^{(o)}(\mathbf{x},\mathbf{y}_\omega,\mathbf{y}_{\omega+1})$ signifies the set of time-coupling constraints, representing the volumetric balance for the solvent tanks given by Eqs. 4ab-4ag, as well as the ramping constraints of the power plant denoted by Eqs. 4g-4i, 4n, and the ramping constraints of the capture system given by Eqs. 4w-4x. From model M1, parameter vector $\mathbf{k}_\omega$ comprises of the spot-market electricity price π^s_ω and capacity factors of wind and solar PV systems $cf_{w,\omega}, cf_{sp,\omega}$ respectively.

3.2.2 Time aggregation of scenarios.

Time-aggregation of parameter profiles in the first stage of the solution strategy is performed using the SCENRED reduction package[56] in GAMS[57] environment. The workflow of this process is depicted in Figure 3.

To begin with, we first obtain the hourly discretized parameter vector $\mathbf{k}_\omega = (\pi^s_\omega,\ cf_{w,\omega},\ cf_{sp,\omega})$ using data from a previously observed year. This data is recast into a scenario tree with the branches denoting the time steps or the different scenarios. Each branch consists of three nodes, representing the three parameters constituting vector $\mathbf{k}_\omega$. For the original scenario tree, we have $NS = h^{op}$ scenarios and equal frequency of each scenario occurrence. Using Eq. 1, the scenario frequency can be derived as:

$$p_\omega = \frac{1}{h^{op}}, \quad \forall \omega \in \Omega. \tag{8}$$

The developed scenario tree, as illustrated in Figure 3, with the node data and frequencies for each branch is given as an input to the SCENRED tool. The desired reduction accuracy is specified as 94% and the algorithm to be backward reduction.[59] To obtain the desired accuracy, the tool eliminates branches corresponding to similar parameter values and generates a smaller scenario tree with fewer branches. The frequencies are then reassigned among the preserved scenarios with the deleted branches assigned zero frequencies. The set of reduced scenarios is denoted by: $\Omega' \subseteq \Omega$, with p^r_ω denoting the updated frequency of scenario $\omega \in \Omega'$. Furthermore, the reduced scenario tree may not maintain the property of equal scenario frequencies of the original tree. The node data for the preserved branches along with the updated frequencies p^r_ω is used to obtain the time-aggregated parameter profiles, with the time-weightage of each scenario calculated as:

$$t^r_\omega = p^r_\omega h^{op}, \quad \forall \omega \in \Omega'. \tag{9}$$

3.2.3 Overall algorithm.

The reduced scenario set is then used to solve the NPV maximization model in the general form M0 to obtain the complicating design decisions $\mathbf{x}$. These decisions are fixed and the second-stage problem, represented by Eqs. 6a, 6d-6f of M0, is then solved using the original scenario set Ω to obtain the optimal operational decisions $\mathbf{y}_\omega$. This two-stage optimization framework decouples the first-stage and second-stage decisions, thereby providing computational advantages without compromising on the solution quality. The entire workflow of the solution strategy combined with the scenario reduction process is given in Algorithm 1. The implementation of the algorithm for a sample power plant is also included on our GitHub repository: `https://github.com/manali-zantye/renewables_fcc`. This demonstrates the various steps of the optimization algorithm in detail.

We demonstrate this framework through case studies on power plants in a single state as well as across the nation in the United States. For the two case studies, we further consider two different

Algorithm 1: Two-Stage Optimization through Scenario Reduction

Step 0: Obtain hourly-discretized data for $\pi^s_\omega, v_{w,\omega}, H_\omega$ from a full representative year.
Step 1: Apply Eqs. 2-3 to obtain parameter vector $\mathbf{k}_\omega = \left(\pi^s_\omega,\ cf_{w,\omega},\ cf_{sp,\omega}\right)$, with frequency p_ω given by Eq. 8.
Formulate the original scenario tree.
Step 2: Specify desired scenario reduction accuracy.
Step 3: Perform time-aggregation via scenario reduction using SCENRED.
Obtain the following attributes from the reduced scenario tree: $\Omega' \subseteq \Omega$ and p^r_ω. Calculate t^r_ω using Eq. 9.
Step 4: Solve overall model M0 using Ω' and t^r_ω to obtain the optimal design decisions $\mathbf{x}^*$.
Step 5: For the second-stage problem given by Eqs. 6a, 6d-6f, fix $\mathbf{x} = \mathbf{x}^*$.
Solve using data from the original scenario set Ω, with frequency p_ω, to obtain the optimal operating decisions $\mathbf{y}^*_\omega$.

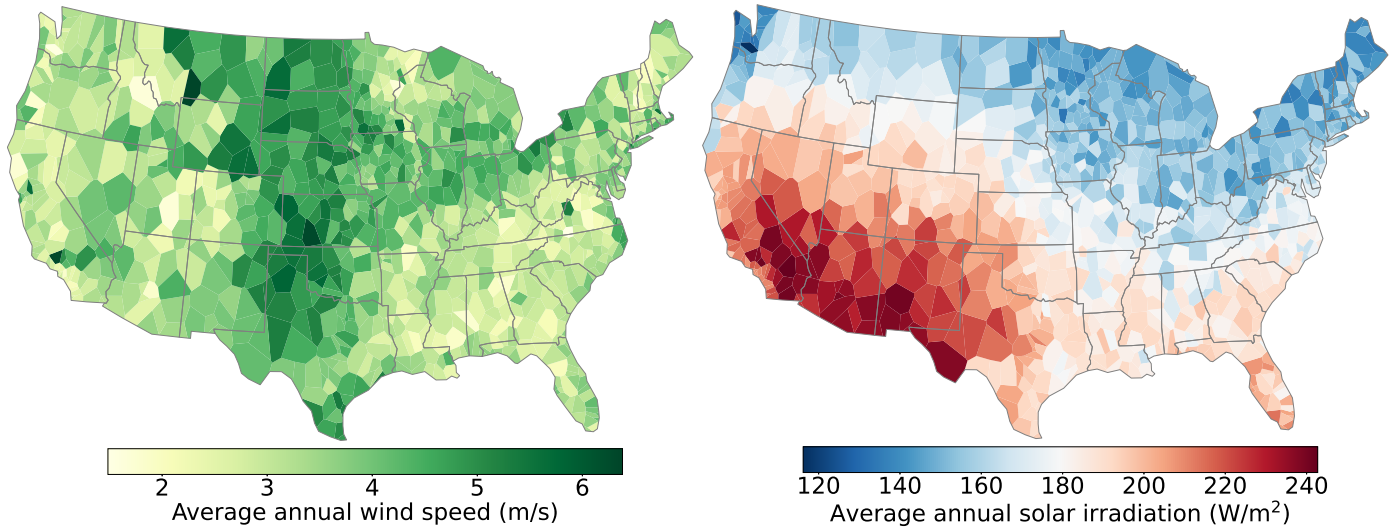

(a) Wind speed.

(b) Solar irradiation.

Fig. 4 Nationwide variation of renewable resource availability in the US. Hourly-discretized data is obtained from NREL's National Solar Radiation Database (NSRDB) for 1020 Typical Meteorological Year (TMY3) sites.[58] The dataset represents the typical weather conditions in any location, derived based on historical observations for the past 30 years. Voronoi polygons are used to depict the variation of annual average data, where each polygon represents the data for a single weather station and the area covered by the polygon is closer to that station as compared to any other. The wind speed data suggests that the Midwest region of the US is potentially suitable for wind integration with power plants. On the other hand, the Southwest region has abundant solar energy. The integration of power plants with such geographically distributed energy resources requires optimization-based informed decision-making.

cases for optimization, current and future, defined by the cost of renewables and the cost of emitting CO_2 to the atmosphere. Table S4 of the ESI shows the specific cost values for the current and future cases.† We present the optimization results in the form of addressing the research questions listed in Section 1.

4 Results: Nationwide integration

Hourly-discretized data for wind speed $v_{w,\omega}$ and solar insolation H_ω across the nation is obtained from NREL's National Solar Radiation Database (NSRDB) for 1020 Typical Meteorological Year (TMY3) sites.[58] The TMY dataset constitutes a full year of time-series data based on historical observations for the past 30 years and is representative of the typical weather conditions in a location. Figure 4 shows the nationwide variation of the yearly average wind speed and solar radiation intensity.

As expected, the highest solar resource availability is observed in the Southwest part of the US and the lowest in the Northeast. On the other hand, the Midwest region exhibits the highest wind speeds. The corresponding capacity factor of wind turbines and solar PV is determined using Eqs. 2-3. Figure 5a-5b shows the nationwide variation of the annual average of the capacity factors. We observe that the capacity factor for wind turbines exhibits a larger range of variation as compared to the variation in capacity factor of solar PV systems. Additionally, the capacity factor of solar PV is on an average higher as compared to wind turbines.

Furthermore, data for coal power plants across the nation is acquired from the United States Environmental Protection Agency (EPA)'s Emissions & Generation Resource Integrated Database.[62] Owing to tighter emission regulations and poor cost competitiveness as compared to other generating resources, about 50 GW coal-fired capacity in the US was retired between 2010 to 2019, 14.3 GW had the boiler repurposed to burn natural gas, and 15.3 GW capacity was entirely replaced with natural gas combined cycle (NGCC) plants.[63] There are about 309 operational power plants with coal-based generating units as per EPA's eGRID2018v2 database.

For the 309 operational plants, data for the nameplate capacity is obtained as an input parameter for model M1, p^{max}_{cl}. We

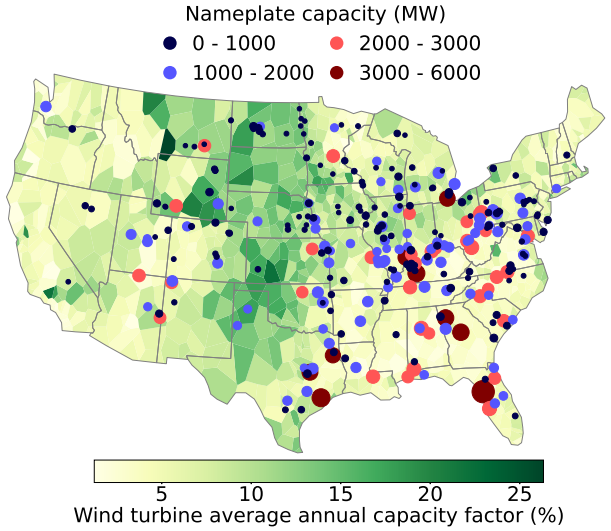

(a) Variation of wind turbine capacity factor and power plant nameplate capacity.

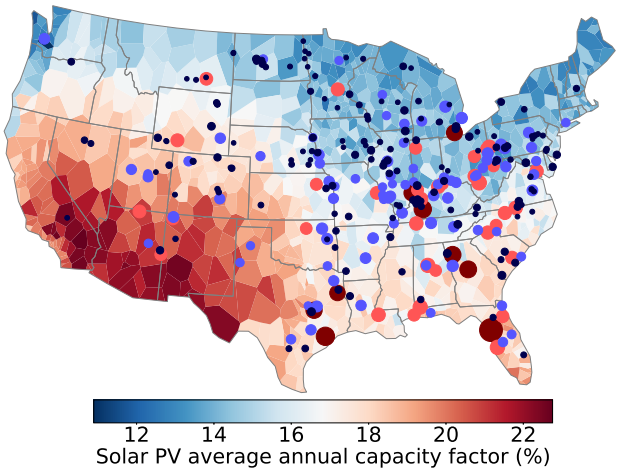

(b) Variation of solar PV capacity factor and power plant nameplate capacity.

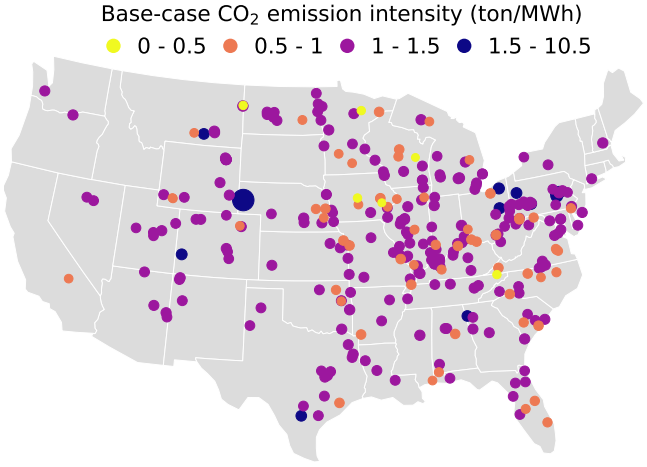

(c) Variation of power plant base-case CO_2 emission intensity.

Fig. 5 Nationwide variation of renewable capacity factors and power plant data. Capacity factors for the 1020 weather stations are shown using Voronoi polygons. The discrete points depict the data for each power plant, with the size proportional to the magnitude of the data represented.

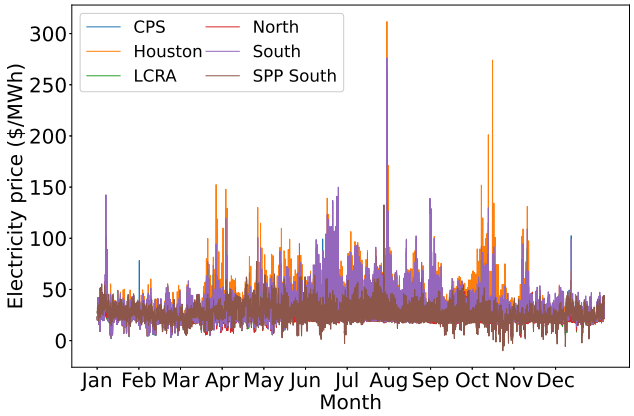

Fig. 6 Annual variation of electricity price for different settlement points in the state of Texas. Hourly discretized data for the representative year of 2017 is shown for 6 load zones in the state: CPS, Houston, Lower Colorado River Authority (LCRA), North, South and Southwest Power Pool (SPP) South.[60,61]

assume that the base-case CO_2 emission intensity, E_{cl}, for each plant is equal to its average annual CO_2 emission rate derived from the database. Moreover, if the plant's primary fuel is coal as per eGRID2018v2, its nameplate capacity and base-case emission intensity are assumed to be the same as that of the entire plant given in the database and not specifically for its coal generating units alone. This is because the emission intensity of individual generating units is not provided and since coal is the primary fuel of the plant, majority of its production capacity and CO_2 emissions can be attributed to the use of coal.

Figure 5a-5b also depict the power plant locations and their nameplate capacities. Majority of the plants (around 57%) have a nameplate capacity below 1000 MW. We also observe a small fraction of plants (less than 3%) with large capacities above 3000 MW. Weather data for each power plant is derived from the weather station in its closest proximity using the Haversine formula for spherical distance, or the data for the Voronoi polygon it falls into. Figure 5c shows the base-case CO_2 emission intensity of the power plants. Nearly 97% of the plants have emission intensities within the range of 0.5-2 ton MWh^{-1}. High emission intensities, above 2 ton MWh^{-1}, are observed for power plants with capacities less than 100 MW. The nationwide average emission intensity is around 1.11 ton MWh^{-1}.

It is difficult to obtain publicly available data of electricity price for all power plants, especially those which fall under the purview of traditional wholesale electricity markets. These markets, which typically exist in the Southwest, Southeast and Northwest involve vertically-integrated utilities responsible for the generation, transmission and distribution of electricity to the customers.[64] Owing to the limited data and the difficulty associated with deriving data for each power plant separately, we assume a fixed price profile for the nationwide case study. As the electricity price profiles in the statewide case given in Figure 6 do not exhibit significant variation over the different settlement points, we also extrapolate this to the nationwide case and derive the fixed profile by taking the average price from the statewide case over all the settlement

points. The data used to derive this price profile is included on the following GitHub repository link:https://github.com/manali-zantye/renewables_fcc. The data for the weather stations and power plants are also included here.

Using scenario reduction, the number of scenarios are significantly reduced from 8760 to be in the range of 50 to 70 for all the plants, while retaining 94% accuracy. Depending on the number of scenarios, the number of equations and variables in Step 4 of the two-stage optimization algorithm given in Section 3.2.3 vary in the range of 3000-4500. The number of equations and variables in Step 5 of the algorithm is the same for all the power plants: 534,371 and 551,905 respectively. The MILP model of Step 4 and the LP model of Step 5 are solved using BARON[65] v. 20.4.14 in GAMS[57] environment with a resource limit of 48 hours. The resulting optimality gap in Step 4 ranges between 0.01%-25%. On the other hand, the optimality gap for Step 5 is 0.01% for all the power plants.

The optimization results for the two cost scenarios are presented below. The current cost scenario is representative of the latest cost estimates for renewable systems and the present carbon pricing landscape. On the other hand, the future case characterizes projected estimates of reduced renewable energy cost and the carbon pricing incentive required to cost-effectively transition to a low-carbon energy sector. How soon we can get to these estimates will depend on future policies and carbon pricing strategies. For instance, one of the several federal tax proposals pending in the US Congress projects the increase in CO_2 tax to \$80 per ton by 2024.[66,67] The CO_2 selling price of \$35 per ton is based on the projected increase in the 45Q Credit for carbon capture, storage and utilization projects through 2026.[68] On the other hand, increasing economies of scale and technological advancements can drive the reduction in solar/wind investment cost to \$0.3 per Watt over the next two decades.[69]

4.1 Is it profitable for a coal power plant to invest in the integrated system to reduce CO_2 emissions?

Owing to the high cost of renewables and low incentive to reduce CO_2 emissions in the current cost scenario as given in Table S4 of the ESI,† the optimal solution indicates that it is uneconomical to integrate either a CO_2 capture system or a renewable energy farm with any of the 309 coal power plants across the nation. In the absence of the additional investment, the cost of electricity generation (COE), or the optimal operating cost of generating 1 MWh of electricity, is given by

$$COE = \frac{\sum_{\omega \in \Omega} t_\omega \; Cost_\omega{}^*}{\sum_{\omega \in \Omega} t_\omega \; P^{in}_{g,\omega}{}^*}, \tag{10}$$

where the optimal power input to the grid $P^{in}_{g,\omega}{}^*$ equals the power output from the stand-alone coal plant $P^{out}_{cl,\omega}{}^*$. The optimal cost $Cost_\omega{}^*$ includes the operational cost components of the coal plant i.e. the variable O&M cost including the cost of fuel, tax paid on CO_2 emissions and power plant ramping cost. Figure 7a shows the variation of the COE with the base-case CO_2 emission intensity of the power plants, excluding the outlier data point with emission intensity greater than 10 ton MWh^{-1}. As can be seen from Figure 7a, the cost of electricity generation varies between \$33.6-53.4 per MWh and shows an increasing trend with increas-

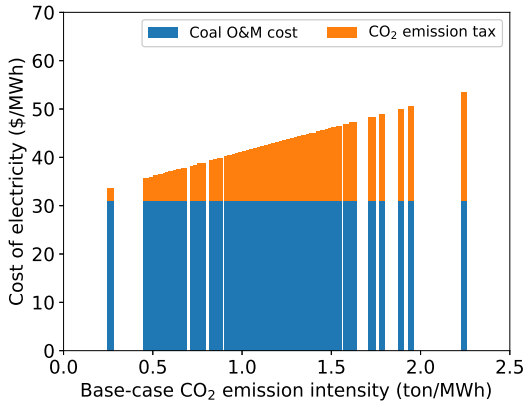

(a) Cost of electricity versus base-case emission intensity.

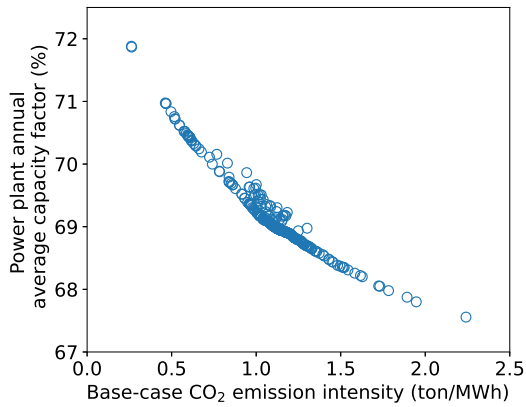

(b) Capacity factor versus base-case emission intensity.

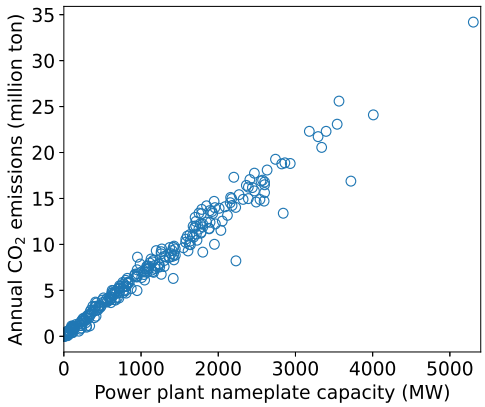

(c) Annual emissions versus nameplate capacity.

Fig. 7 Power plant cost, capacity factor and CO_2 emissions for the current cost scenario. Due to the low economic incentive, the integration of emission reduction techniques such as CO_2 capture or renewable integration is economically unfavorable. The operating cost portion of the total cost is constant at \$31 per MWh. In the absence of emission abatement schemes, a higher cost on emissions is incurred for increasing base-case emission intensity. This also results in lower utilization of coal power at higher base-case intensities. The total annual emissions increase with the size of the power plant.

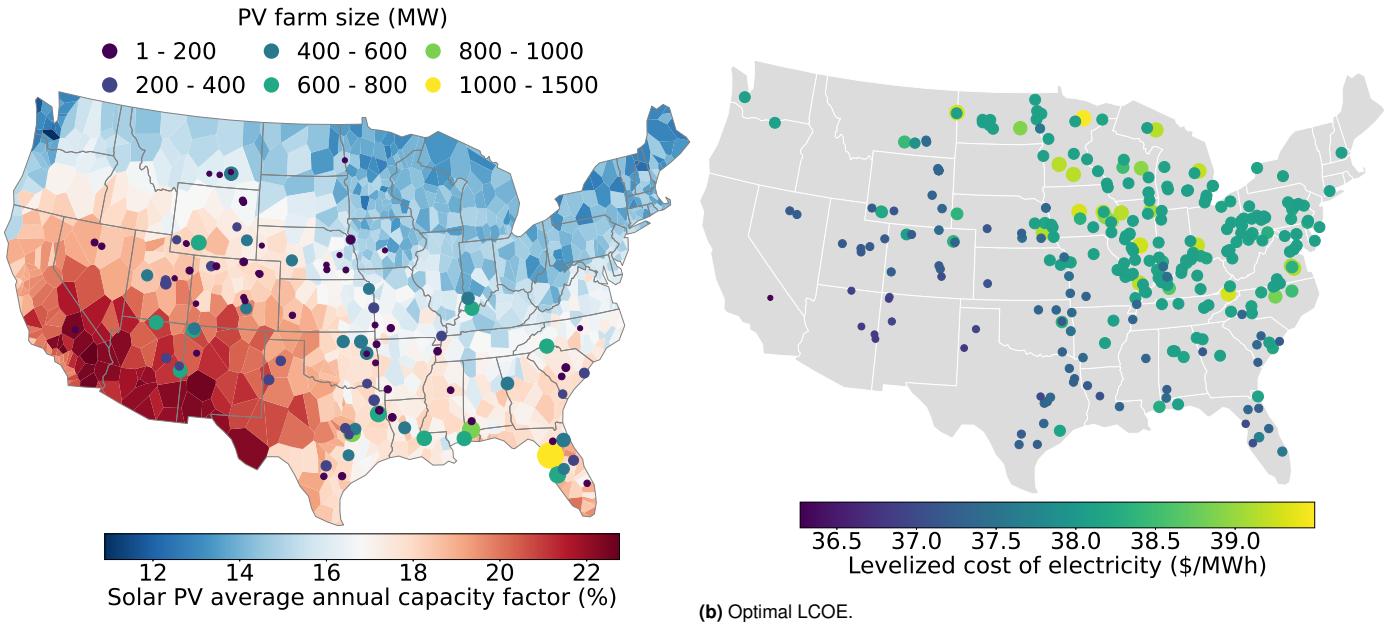

(a) Optimal co-located solar PV farm size.

(b) Optimal LCOE.

Fig. 8 Nationwide variation of system design and cost for the future cost scenario. The high economic incentive facilitates the installation of emission reduction techniques in existing coal plants. The integration of solar PV is optimal for one-third of existing coal plants in the US, with CO_2 capture retrofit optimal for all 309 plants. Solar-assisted CO_2 capture is selected predominantly in regions with average solar capacity factors above 16%. The solar farm size is below 200 MW for a majority of the plants. The corresponding LCOE for the integrated system falls between $36-40 per MWh, with lower LCOE observed for plants with solar energy integration.

ing base-case emission intensity due to the increasing tax paid on CO_2 emissions. The O&M cost associated with coal power generation forms a major component of the total cost and is constant at C_{cl}^{gen} as can be validated from Eqs. 4f and 10. The power plant ramping cost is relatively insignificant as compared to the other cost components.

The average annual capacity factor of the coal power plant, or the percentage utilization as compared to its maximum installed capacity is determined using

$$cf_{cl}^{avg} = \frac{\sum_{\omega \in \Omega} t_\omega \; P_{cl,\omega}^{out\,*}}{p_{cl}^{max} \; h^{op}}. \tag{11}$$

The average annual capacity factor ranges between 66.7%-71.9% and shows a decreasing trend with increasing base-case emission intensity as depicted in Figure 7b. On the other hand, in the absence of a capture system to reduce emissions, the annual emissions from the power plants increase with the plant size, as shown in Figure 7c.

The optimization results for the projected future cost of renewables and CO_2 emissions suggest the integration of solar PV with 102 plants of the 309 power plants in the nationwide case, with CO_2 capture retrofit selected for all the power plants. Wind energy installation as well as an electric boiler to convert electricity from renewables to steam energy for use in CO_2 capture is not selected for any of the 309 plants.

Wind energy integration is not optimal due to lower average capacity factors as compared to solar. The electric boiler is not chosen in the optimal solutions, mainly due to its high investment cost, which is nearly 30% of the solar/wind energy cost in the future cost scenario. Additionally, the equivalent thermal-to-electric power requirement of the solvent regeneration reboiler is equal to the combined electric power requirement of the auxiliary equipment and CO_2 compressor in the capture system. Thus, it is optimal to avoid an additional investment for the electric boiler and solar power is used for CO_2 capture only to meet the electric power requirement of the auxiliary equipment and compression system. Although the energy required for the CO_2 reboiler comes entirely from the existing coal plant, the solar farm compensates for the reduced power output of the plant by delivering a majority of its power output to the grid. This operational aspect will be discussed in more detail in further sections.

Figure 8 shows the variation of the optimal size of the co-located solar PV farm across the nation for coal plants where solar energy is selected. It can be seen that the solar energy is selected mainly at locations with high annual average capacity factors, particularly in the southern regions. There is little or no solar integration with coal power plants in the northeast regions with lower average PV capacity factors.

Furthermore, a sensitivity study for the reference case power plant with capacity of 600 MW is performed to analyze the variation of system profitability with different levels of CO_2 tax and selling price for the future renewables cost scenario. We have included the analysis in Section S3 of the ESI.† In the absence of a significant CO_2 tax and CO_2 selling price, there would be no economic drivers for investing in a CO_2 capture/renewable system even for a futuristic low renewables price. Figure S1 shows that for a CO_2 tax below $5 per ton and a CO_2 selling price below

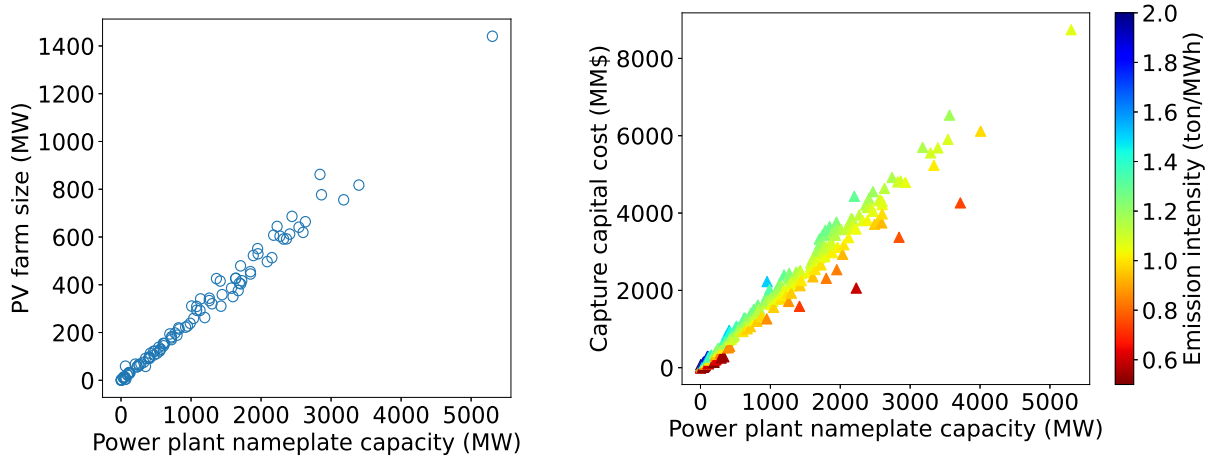

(a) PV farm size versus power plant nameplate capacity.

(b) CO_2 capture system capital cost versus power plant nameplate capacity and base-case emission intensity.

Fig. 9 Optimal integrated system size for the future cost scenario. The optimal solar farm size increases linearly with the coal plant nameplate capacity, with the average being 25.8% of the coal plant capacity. The optimal size of the CO_2 capture system increases with both the coal nameplate capacity and the base-case emission intensity.

$35 per ton, there is not enough economic incentive to reduce emissions from the coal power plant and integrate either a CO_2 capture system or a solar PV farm. The power generation would rely entirely on the coal plant and all the CO_2 produced would be emitted to the atmosphere. Inclusion of a high tax, on the other hand, would drive the integration of both the CO_2 capture and renewables system with the coal plant to reduce emissions. However, the tax paid on the 10% emissions not being captured would add to the cost, which could result in a net loss. A combination of high selling price and a high tax would thereby be necessary to ensure investment in emission reduction techniques and at the same time ensure that the system is profitable. Specifically, we observe that all combinations of CO_2 tax above $55 per ton and CO_2 selling price above $35 per ton favor both CO_2 capture and solar PV integration with the coal plant. To summarize, both the CO_2 tax and the CO_2 selling price would play an important role to incentivize carbon abatement technologies.

4.2 What is the optimal design of the integrated system under spatiotemporal variability in electricity price and renewable availability?

Figure 8 shows that the majority of the solar PV farms integrated with coal-based units for the future cost scenario have a capacity below 200 MW. Figure 9a displays the variation of the solar PV farm size with power plant nameplate capacity for plants where solar energy is selected in the future cost scenario. It can be seen that the optimal solar farm size shows a positive linear correlation to the power plant nameplate capacity. On an average, the solar farm size is 25.8% of the power plant nameplate capacity. Figure 9b shows the capture system capital cost variation with the power plant nameplate capacity and base-case emission intensity. As expected, the capital cost and thereby the capture system size increases with the nameplate capacity of the plant. For power plants with similar nameplate capacities, the capture system size is greater for plants with a higher emission intensity.

4.3 How does the integrated system cost compare with that of a new natural gas plant?

Due to their high CO_2 emissions and significant operating costs, coal plants in the US are being increasingly decommissioned or replaced with the relatively cleaner and cheaper natural gas-fired units. To assess the economic viability of investment in the integrated system for coal power plants as compared to their replacement with natural gas units, we use the levelized cost of electricity (LCOE). It is typically signified as the ratio between the net present value of the projected costs of the additional investment and the discounted energy delivered by the system. In this case, LCOE represents the revenue required per unit of energy generation to recover the cost of building and operating the co-located renewable energy farm and/or the CO_2 capture unit. It is post-calculated based on the optimization solution as follows:

$$LCOE = \frac{CC^{tot*} + DF \sum_{\omega \in \Omega} t_\omega \left(Cost_\omega{}^* - M_\omega^{capt*} \, \pi^{csp} \right)}{DF \sum_{\omega \in \Omega} t_\omega \, P_{g,\omega}^{in}{}^*}, \quad (12)$$

where, DF denotes the discount factor given by:

$$DF = \frac{1}{r^{disc}} - \frac{1}{r^{disc} \left(1 + r^{disc}\right)^{t^{lf}}}, \quad (13)$$

and $CC^{tot*}, Cost_\omega{}^*, M_\omega^{capt*}$ and $P_{g,\omega}^{in}{}^*$ indicate the optimal values of the capital cost, operational cost, amount of compressed CO_2 from capture system and the integrated system's power output to grid respectively. Figure 8 depicts the variation of the optimal LCOE across the nation for the future cost scenario. We observe that the LCOE for all the power plants is below $40 per MWh. Figure 10a further shows that lower LCOE is obtained for power plants with solar energy integration. The nationwide average re-

duction in LCOE from both solar integration and CO_2 capture retrofit is 2.36% as compared to that with capture retrofit alone. As the LCOE associated with the installation of a new NGCC power plant is \$40 per MWh,[70] investing in a solar-powered CO_2 capture unit for the existing coal plant could be economically advantageous as compared to its entire replacement with a new NGCC plant.

Variation of the different cost components constituting the LCOE is shown in Figure 10b. It can be observed that with increasing base-case emission intensity, the CO_2 emission tax, CO_2 T&S cost and the total capital cost of the integrated system show an increasing trend. However, the increasing cost is compensated by the additional revenue generated by the system due to the sale of captured CO_2 in the carbon market. Considering the solvent loss of MEA to be 1.5 kg ton^{-1} of captured CO_2 and a cost of \$1 per kg,[71,72] the average cost incurred due to solvent loss would be only 4.75% of the total system cost. Thus, the negligible cost from solvent loss is not reported in the overall costs.

Furthermore, Figure 10c depicts the overall percentage reduction in the base-case CO_2 emission intensity of the coal power plants resulting from the integration. We observe that the overall emission intensity reduction achieved is between 87.5-91% for all the power plants. The average reduction in emission intensity achieved in plants with CO_2 capture retrofit without solar integration is nearly 87.7%. Additionally, a 0.75% higher average reduction in emission intensity is observed for plants with both solar integration and capture retrofit. Thus, overall higher emission intensity reduction is obtained from integration as compared to the 60% reduction achieved if the coal plant is replaced with a natural gas unit.[73] This indicates that it is more economical and beneficial for the coal plant operators to invest in the integrated system of CO_2 capture and renewable energy in a scenario with a high price on carbon emissions and low renewable energy cost, as compared to replacing the coal-fired unit with a NGCC plant to obtain reduced emissions.

On the other hand, natural gas is also used to provide energy for carbon capture installation in coal plants, a well-known example of which is the Petra Nova CO_2 capture facility. Although a natural gas system requires less investment cost and is more reliable as compared to renewables, it adds to the overall CO_2 emissions and undermines the benefits obtained from CO_2 capture. For instance, during the period of January 2017 to May 2018, Petra Nova reportedly captured 1.7 million ton of CO_2. However, emissions from the co-located natural gas unit amounted to nearly 450,000 ton, reducing the net CO_2 captured to 1.25 million ton.[74] To further demonstrate the benefits of our integrated system, we compare the cost and emission intensity of such a natural gas-fired capture unit with the solar-powered CO_2 capture retrofit.

For this analysis, we assume that the existing coal power plant is retrofitted with a CO_2 capture system and a co-located NGCC plant, in place of the co-located solar PV field. We restrict this analysis to the 102 power plants for the nationwide case where solar PV is selected. Furthermore, we assume that the total power output of the natural gas plant over a year is the same as the total solar output at each location:

$$\sum_{\omega\in\Omega} t_\omega \; {P^{out}_{ng,\omega}}^* = \sum_{\omega\in\Omega} t_\omega \; {P^{out}_{sp,\omega}}^* \tag{14}$$

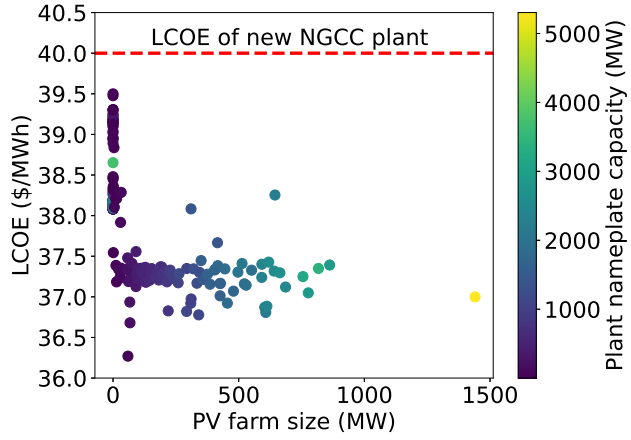

(a) Optimal LCOE versus solar farm size.

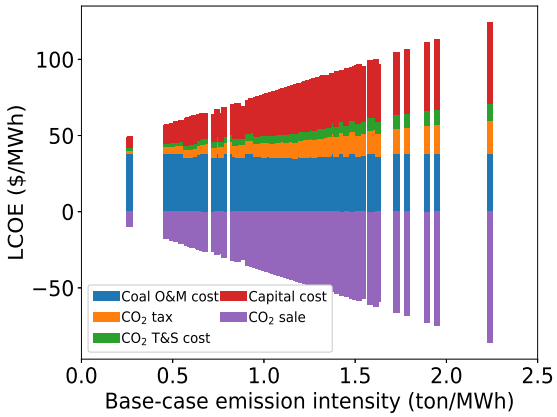

(b) LCOE breakdown versus base-case emission intensity.

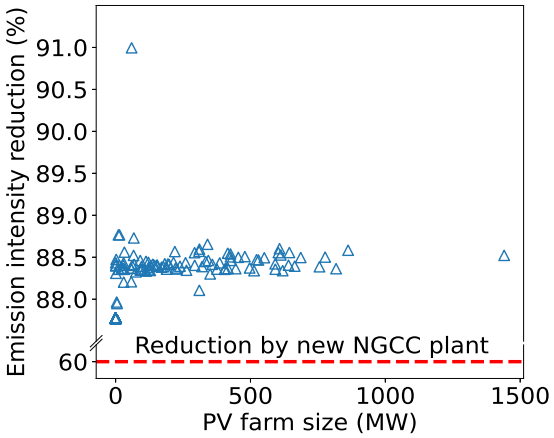

(c) Reduction of emission intensity versus solar farm size.

Fig. 10 Integrated system cost and emission intensity for the future cost scenario. The LCOE from integrating the coal plant with solar-assisted CO_2 capture is lower and the emission reduction obtained is higher as compared to the case where the coal plant is replaced with a new NGCC plant. The capital cost, CO_2 tax and CO_2 transportation cost of the integrated system increase with the base-case emission intensity. This high cost is offset by the revenue generated from the carbon market through the utilization of captured CO_2.

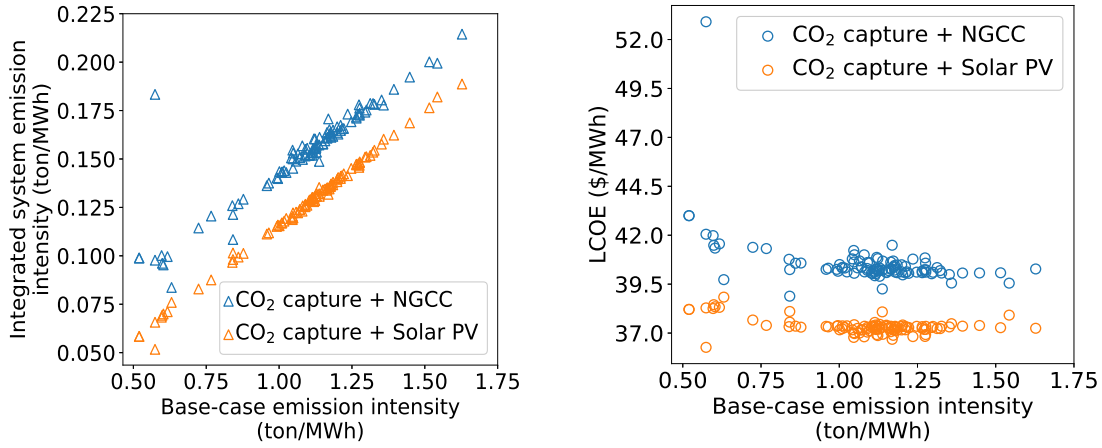

(a) Integrated system emission intensity.

(b) Integrated system LCOE.

Fig. 11 Comparison of the emission intensity and LCOE of solar-powered CO_2 capture with NGCC-powered CO_2 capture integration in coal plants for the future cost scenario. Both the emission intensity and LCOE for the integrated system with NGCC-powered capture is observed to be higher than with solar-powered capture. The LCOE decreases with emission intensity due to the higher revenue obtained from the carbon market at higher emission intensities. The outlier point with an emission intensity of 0.183 ton MWh^{-1} and LCOE of \$53 per MWh is for the power plant with the co-located solar PV field size 95% of coal nameplate capacity. Replacing such a large solar field with an NGCC plant of the same power output results in a large amount of natural gas-based emissions and a high LCOE due to CO_2 tax.

Considering a levelized cost $LCOE_{ng}$ of \$40 per MWh for the NGCC plant with a CO_2 emission intensity E_{ng} of 0.5 ton MWh^{-1},[73] the total levelized cost $LCOE'$ of the coal-CO_2 capture-NGCC integrated system is given by:

$$LCOE' = LCOE - \frac{CO_{sp}\ sz_{sp}^*}{DF \sum_{\omega\in\Omega} t_\omega\ P_{g,\omega}^{in\ *}} + \frac{LCOE_{ng} DF \sum_{\omega\in\Omega} t_\omega\ P_{ng,\omega}^{out\ *}}{DF \sum_{\omega\in\Omega} t_\omega\ P_{g,\omega}^{in\ *}} + \frac{C^{em} E_{ng} DF \sum_{\omega\in\Omega} t_\omega\ P_{ng,\omega}^{out\ *}}{DF \sum_{\omega\in\Omega} t_\omega\ P_{g,\omega}^{in\ *}}, \quad (15)$$

where $LCOE$ is the levelized cost of the coal-capture-solar PV integrated system given by Eq. 12 and C^{em} is the CO_2 emission tax of \$80 per ton. To obtain the levelized cost of the coal-CO_2 capture-NGCC integrated system, we first subtract the solar PV capital cost portion from the levelized cost of the coal-CO_2 capture-solar PV system. The capital and operating costs of the NGCC plant as well as the tax paid on natural gas emissions are added, as given by the third and fourth terms of Eq. 15.

Figure 11 depicts the variation of emission intensity and LCOE for the solar-powered and natural gas-powered CO_2 capture for the 102 plants studied. We observe that the CO_2 emission intensity of the integrated system with NGCC is higher than that with solar integration. On an average, we obtain 3.1% lower emission intensity reduction of the coal plant from natural gas-fired capture as compared to solar-powered capture retrofit. Although the levelized capital cost of the co-located NGCC plant alone is comparable to the future cost of solar PV, the total levelized cost of the integrated system is on an average 8.6% higher with NGCC due to the carbon footprint of natural gas-based generation and the associated carbon tax.

4.4 To what extent can renewables reduce the cost of CO_2 capture? Can CO_2 capture effectively counter renewable intermittency?

Figure 12 shows the optimal operational profiles of the coal power plant with the highest nameplate capacity and integrated solar farm size in the future cost scenario. The profiles shown are for a representative day in summer, corresponding to the maximum power output of the solar PV farm. It can be seen from Figure 12a that during periods with low electricity price and excess solar energy availability, a major portion of the solar output is directed to the CO_2 capture system. In the absence of an electric boiler to convert solar-generated electricity to steam for use in the desorption unit of the capture system, the solar energy is used to meet the auxiliary energy requirement of CO_2 capture. This auxiliary requirement stems from the electricity requirement of the CO_2 absorption and compression units. Figure 12b depicts the distribution of coal power generated among the various energy sinks. We observe that the coal power plant operates at maximum capacity almost throughout the day, especially during periods with low solar energy production. The coal power in excess of the contract power requirement is used to meet the energy requirement of CO_2 capture during periods of low prices, primarily in the desorption unit.

Figure 12c shows the schedule of capture system operation, i.e. the variation of $r_{a,\omega}$ and $r_{d,\omega}$. It can be seen that the capture system operates at its maximum rate during periods of excess energy availability and low electricity prices. The capture system operation is turned down to provide more energy to the grid when electricity prices are high and solar power is scarce. For instance, due to the decrease in available solar power which supplies part of the energy required for CO_2 compression, and the high electricity price between hours 16-19, the rate of CO_2 desorption and compression decreases during these hours. Taking

advantage of the drop in electricity price at hour 20, the system ramps up the energy-intensive CO_2 desorption and compression process. As there is no solar power available at hour 21 and due to the spike in price, the desorption/compression rate drops to zero. Thus, the capture system and renewable energy system operate synergistically to attain reduced emissions: the excess renewable energy can be used to meet the high energy requirement of CO_2 capture, and the capture system acts in the form of an energy 'storage' medium to counter renewable intermittency.

Figure 13 shows the distribution of energy between the solar energy farm and CO_2 capture unit for plants where both systems are selected in the future cost scenario. From Figure 13a, we can observe that the amount of the total solar power output delivered to the grid is greater as compared to that used in CO_2 capture. This is because the reboiler power, which constitutes a majority of the capture system power requirement is derived from the coal power plant in the absence of an electric boiler. The nationwide average of the fraction of solar output used in capture is around 36.5%. On the other hand, Figure 13b shows the reduction in CO_2 capture energy intensity and thereby the capture cost resulting from the use of solar energy directed to the capture system. Here, we observe the overall capture system cost reduction using solar power falls between 4%-14%, with the average being around 8.9%.

The ratio of solar PV farm size to the coal power plant nameplate capacity in Figure 13 shows little spread around the average value of 25.8%. This can be explained from the result shown in Figure 9a, where the optimal solar farm size linearly increases with the power plant nameplate capacity at the nationwide scale, with the average size being 25.8% of the coal capacity. Despite the little spread of this ratio, it is an important output that influences both the percentage of solar energy used in CO_2 capture as well as the CO_2 capture cost reduction using solar energy. As shown by Figure 13a, the fraction of solar output directed to CO_2 capture shows a strong negative correlation to the ratio of PV size to the coal nameplate capacity, with a Pearson correlation coefficient of -0.53. Conversely, from Figure 13b, we observe that the fraction of total capture cost reduced using solar energy increases with the relative size of the solar farm as compared to the coal plant, with the computed correlation coefficient being 0.39, indicating moderate correlation.

To further quantify the value of CO_2 capture in addressing renewable intermittency in the future cost scenario, we evaluate the additional capital cost required if the excess solar energy is stored in a battery in place of its use in CO_2 capture. We assume that the excess solar power charged to the battery during the peak solar hours is discharged during the end of the day when limited solar power is available. The battery is thereby assumed to be completely empty during the beginning and the end of a day, making each day independent. Figure 14a displays the annual variation of excess solar energy charged to the battery in a day for the largest solar farm of 1440 MW capacity. The battery size is post-calculated from the optimization results based on the maximum daily excess solar energy which would otherwise be used in CO_2 capture. For the 1440 MW solar farm, this represents the point with around 3917 MWh of excess solar energy in a day in the month of May. The maximum excess energy is selected to give the most conservative estimates of battery size and associated capital cost. Figure 14b represents the variation of the calculated battery size and associated capital cost with the solar PV farm size. It can be seen that there is a strong linear relationship between the equivalent battery cost and the solar field size.

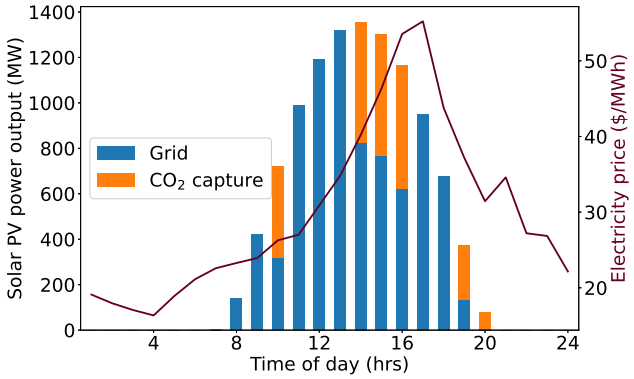

(a) Solar power output distribution.

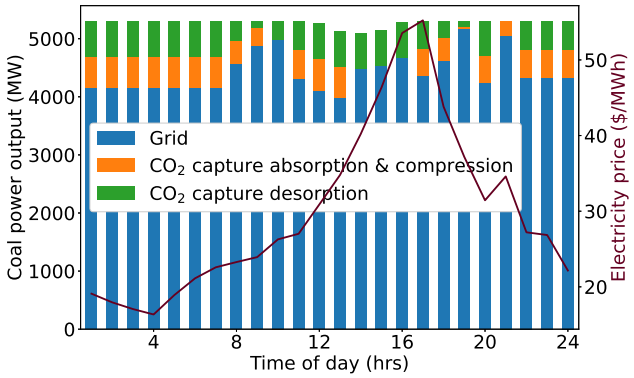

(b) Coal power output distribution.

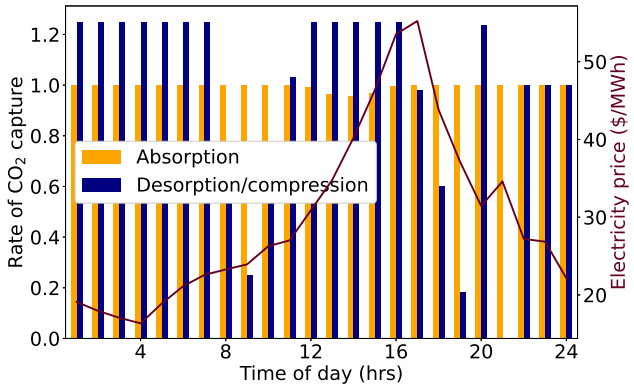

(c) CO_2 capture rate.

Fig. 12 Operational profiles of the integrated system for a summer day for the future cost scenario. Majority of the solar output is delivered to the grid, with excess solar output utilized to provide energy for the CO_2 absorption and compression processes in the capture system. The coal plant operates at maximum output when there is little/no solar power available. During periods of low electricity price, it utilizes excess energy predominantly for CO_2 desorption. The CO_2 capture system ramps up its output during periods of excess solar energy availability and low electricity price.

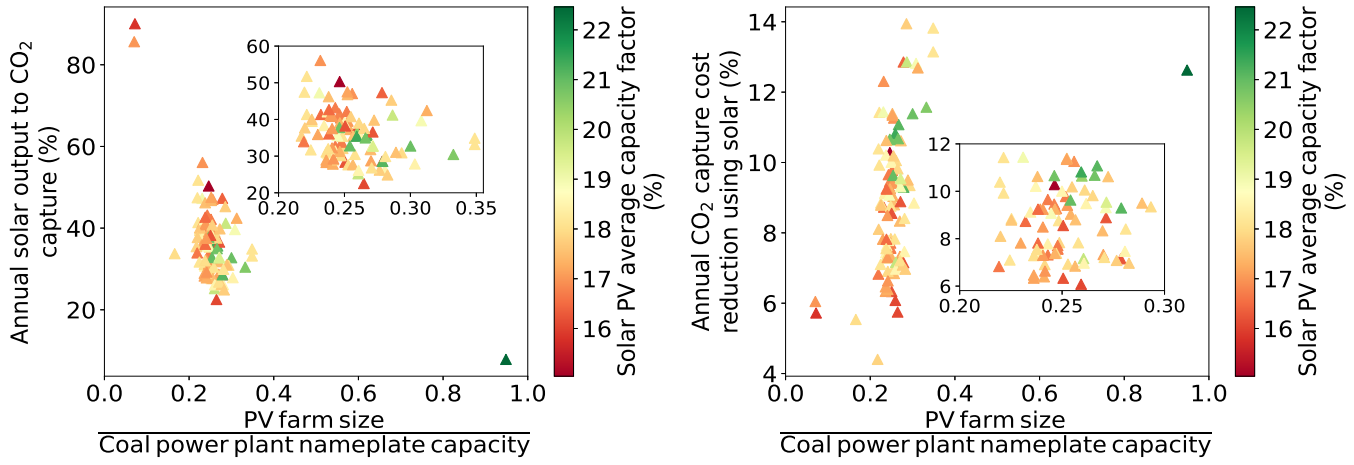

(a) Fraction of solar output used in CO_2 capture.

(b) Reduction of CO_2 capture system cost using solar energy.

Fig. 13 Distribution of energy between the solar farm and CO_2 capture system for the future cost scenario. In the absence of an electric boiler to utilize solar power to meet the steam requirement of CO_2 capture, majority of the solar output is delivered to the grid. On an average, 36.5% of the total solar output is utilized for CO_2 capture and 8.9% of the capture system cost is reduced through solar power. The outliers on the top left of (a) are for locations with average solar capacity factors in the bottom 10% of the nationwide values, resulting in solar PV farm sizes approximately 7% of the coal plant nameplate capacity. Such small farms do not aid much in the supply of power to the grid and the solar output is used almost entirely for CO_2 capture. The outlier on the bottom right of (a) is for the plant with solar average capacity factor in the top 10%, but base-case emissions in the bottom 10% of the nationwide values. This results in the selection of a large solar farm, which delivers a significant amount of its power output to the grid. However, the fraction of reduction in CO_2 capture costs using solar energy for this plant lies close to the nationwide average as shown in (b). The data point for this plant in (b) is displaced horizontally due to the large PV farm size.

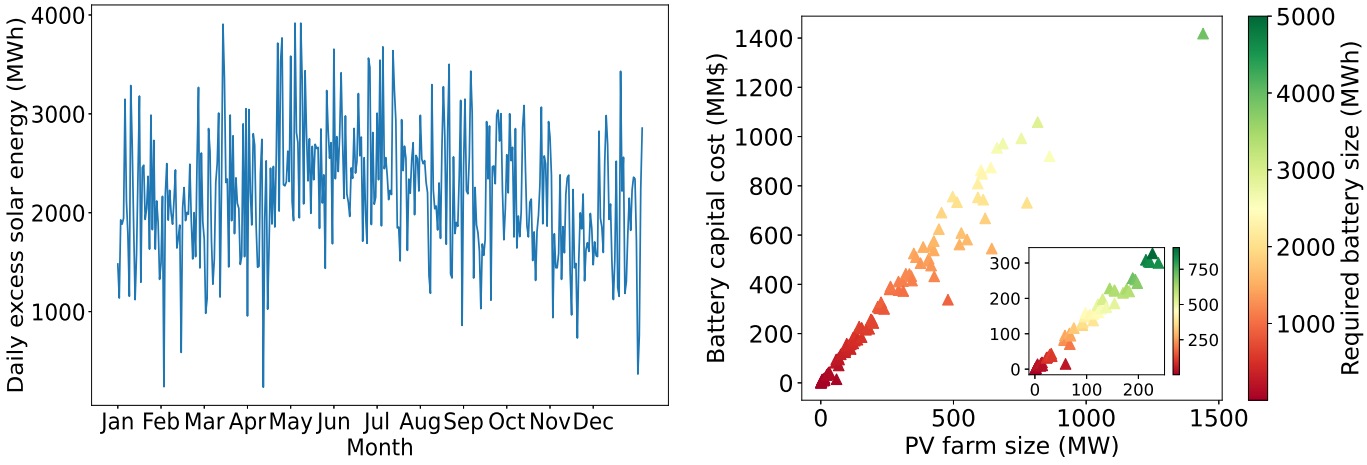

(a) Excess solar energy charged to battery.

(b) Required battery size and capital cost.

Fig. 14 Equivalent battery size required to store excess solar energy for the future cost scenario. To counter renewable intermittency in the absence of the synergistic integration with CO_2 capture, energy storage in the form of a battery would be required to store the surplus solar power. Variation of excess solar energy charged to the battery over a day for a representative solar PV farm is shown in (a). The battery is sized on the basis of the maximum daily excess solar energy. Considering the Li-ion battery type, this translates to a battery capital cost which increases with the solar farm size. The average battery capital cost is 4.4 times the solar farm size. The integrated system thereby avoids this huge investment in battery storage by use of the flexible CO_2 capture process as an indirect energy storage mechanism.

Considering the high-efficiency Li-ion battery type with a 2025 predicted total project cost of $362 per kWh,[75] we obtain the average battery capital cost to be 4.4 times the co-located solar PV farm size. The CO_2 capture system thereby avoids this huge investment while addressing renewable intermittency and directly reducing the CO_2 emissions of the coal power plant.

5 Regional or statewide integration

The focus of the statewide case study is on coal power plants in the state of Texas. Texas is an important state in terms of energy production in the US, being the largest electricity producer and consumer. Additionally, the state has abundant renewable resources and leads the country in wind-powered electricity generation. It also ranked sixth in solar power generation in 2019.[76]

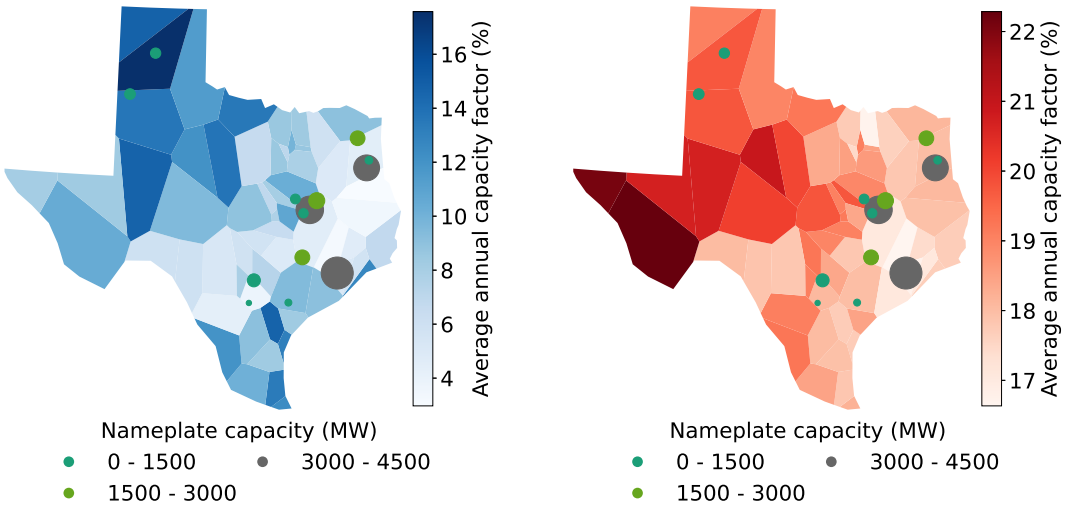

(a) Average wind turbine capacity factor.

(b) Average solar PV capacity factor.

Fig. 15 Statewide variation of renewable capacity factors and power plant data. Weather data for 61 TMY3 sites across the state is displayed using Voronoi polygons. The highest average wind turbine capacity factors are observed in north Texas and the Panhandle region. On the other hand, solar PV has the highest capacity factors in the western region. The discrete points on the plot represent the 14 power plants with operational coal-fired generators, with the point size proportional to the plant nameplate capacity. Majority of the plants have nameplate capacity below 1500 MW.

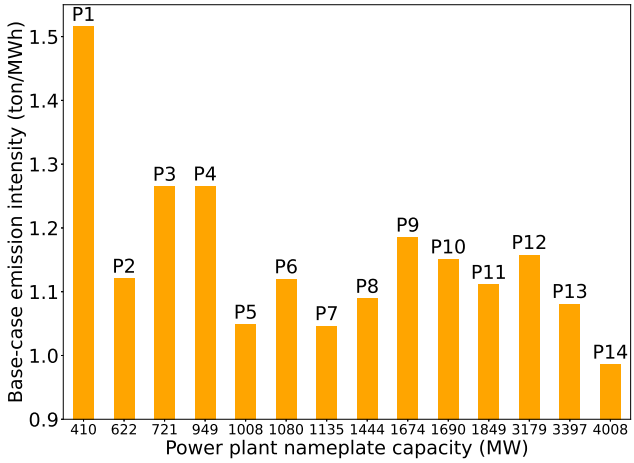

Fig. 16 Variation of power plant base-case CO_2 emission intensity with nameplate capacity for statewide case. Emission intensity of stand-alone power plants without CO_2 capture system installation is depicted. The power plants are denoted as P1-P14 in ascending order of their nameplate capacities.

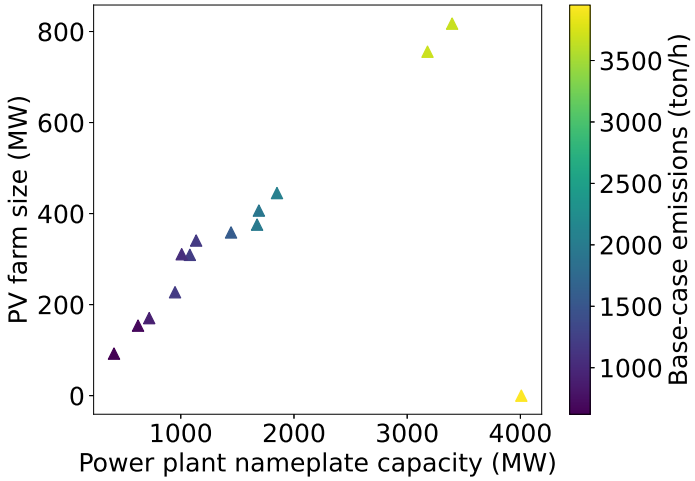

Fig. 17 Co-located solar PV farm size in the state of Texas for the future cost scenario. Integration of solar energy is optimal for all but one power plant (P14) with the lowest solar capacity factor and base-case CO_2 emission intensity. The PV farm size increases with the coal plant capacity and the total base-case emissions. The average farm size is 25.2% of the coal nameplate capacity.

Majority of the coal power plants in Texas fall under the purview of the Electric Reliability Council of Texas (ERCOT), the independent system operator managing about 90% of the state's electric load.[60] Similar to the nationwide case study, full year of hourly-discretized wind speed and solar irradiation data is procured from the NSRDB database for 61 TMY3 sites across the state. Figure 15 displays the variation of the corresponding annual average capacity factors using Voronoi polygons.

There are about 20 operational power plants with coal-based generating units in Texas as per eGRID2018v2. However, 6 of these are in the process of decommissioning their coal generating units or have retired them between the period of 2018-2020 due to high generation costs and poor operational revenue.[77] Among these, the generation capacity of one 871 MW coal plant will be replaced with an IGCC plant with CO_2 capture, additional renewable energy installation and the purchase of an existing natural gas-fired plant.[78] Furthermore, solar-based generation will potentially replace a 470 MW coal plant.[79]

For the 14 operational plants, the nameplate capacity and base-case emission intensity are assumed to be that of the entire plant if coal is the primary generating fuel, similar to the nationwide

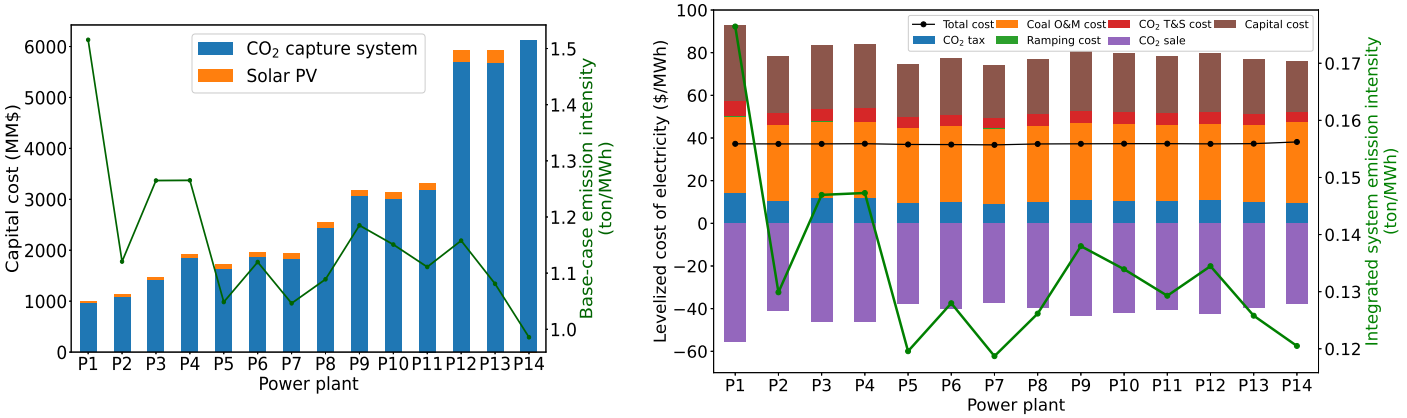

(a) Total capital cost.

(b) System LCOE and emission intensity.

Fig. 18 Integrated system cost and emission intensity for statewide case in the future cost scenario. Analogous to our observation in the nationwide case, the capture system size increases with both the power plant size and emission intensity. Solar PV capital cost is nonzero for all power plants, except for P14 where solar energy integration is not optimal. The integrated system capital cost and carbon tax cost increases with the emission intensity, but this is again compensated by the increasing carbon market revenue.

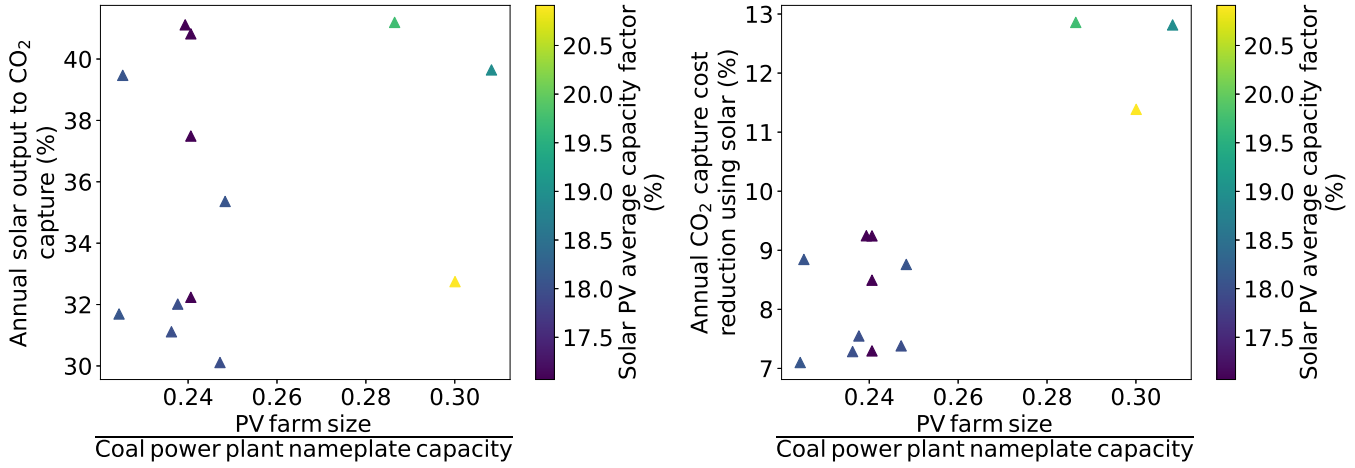

(a) Fraction of solar output used in CO_2 capture.

(b) Reduction of CO_2 capture system cost using solar energy.

Fig. 19 Distribution of energy between solar farm and CO_2 capture system for statewide case in the future cost scenario. Similar to the nationwide case, we observe little spread of the ratio of PV farm size to the coal nameplate capacity around its mean value of 25.2%. Nevertheless, it is an important output, with the percentage of CO_2 capture cost reduced using solar energy showing a strong positive correlation to this ratio. On the other hand, the percentage of annual solar output directed to CO_2 capture shows a weak positive correlation to the relative size of solar farm and coal plant. The statewide average percentage of the solar output used in CO_2 capture is 35%, while the percentage of capture cost reduction using solar energy amounts to 9%.

case. Figure 15 depicts the power plant locations and their nameplate capacities. Majority of the power plants have capacities in the range of 1000-2000 MW, and there a couple of large ones with capacities greater than 3000 MW. Figure 16 displays the variation of the base-case CO_2 emission intensity E_{cl} with nameplate capacity p_{cl}^{max} for the 14 power plants. The CO_2 emission intensity falls in the range of 0.98 to 1.52 ton MWh^{-1}, with the average being around 1.15 ton MWh^{-1}.

Hourly-discretized data for electricity prices, π_{ω}^{s}, is procured from the ERCOT and Southwest Power Pool database [60,61] for the corresponding price hub/load zone the plant falls in based on its location. Of the 14 power plants, P1 and P2 fall in ERCOT's South load zone. Plants P4-P5 and P11-P13 lie in the ERCOT North zone. Plant P8 falls in the CPS zone, P10 in the LCRA zone and P14 in the Houston zone. Moreover, 4 plants: P3, P6-P7 and P9 fall under the purview of Southwest Power Pool's South hub. Figure 6 depicts the variation of electricity price in 2017 for the aforementioned settlement points across the state. The statewide average annual price is $25.8 per MWh.

Figure 17 depicts the optimization results in terms of the variation of co-located PV farm size. A solar PV farm is selected for all the power plants in the future cost scenario except for plant P14 which exhibits the lowest PV capacity factor and CO_2 emission intensity. As noticed in the nationwide case, the renewable energy selection shows a strong positive correlation to the coal plant nameplate capacity, with the solar farm sized at 25.2% of

the coal plant capacity on an average. A divergent observation for the statewide case is the influence of the base-case emissions on the PV farm size.

Figure 18a depicts the variation of the total capital cost for the projected future cost scenario. Similar to the nationwide case, we observe that a CO_2 capture retrofit is selected for all power plants, with the size of the capture system determined by both the nameplate capacity of the plant as well as the base-case emission intensity. Figure 18b shows the corresponding variation of the integrated system's LCOE as well as the emission intensity. As observed in the nationwide case, power plants with higher base-case emission intensity show a higher levelized capital cost along with a higher revenue from the sale of captured CO_2 in the carbon market. The LCOE of all the plants is less than that of a new NGCC plant with an average reduction in the emission intensity of around 88.4%.

The distribution of energy between the solar farm and CO_2 capture unit for the 14 power plants is depicted in Figure 19. The statewide average solar power production used in CO_2 capture system is 35%. However, contrary to the nationwide case, no specific relation is noticed between the fraction of the total solar output used in CO_2 capture and the relative PV farm size or the annual average capacity factor. Figure 19b displays the variation of the fraction of CO_2 capture cost reduction using solar power versus the relative farm size and average capacity factor. Here, we observe that as the size of the solar farm relative to the coal power plant increases, a higher percentage of the CO_2 capture energy requirement is met using solar energy. Also, higher solar availability influences the use of higher amounts of solar energy to reduce capture costs.

6 Conclusions

In this work, we address the challenges of the two pathways for decarbonization, renewable energy and carbon capture, by exploring the synergies between the two technologies. We perform a techno-economic analysis of a power generation system that integrates a coal power plant, a renewable energy field and a flexible CO_2 capture system. To this end, we develop a mathematical programming-based approach to determine optimal integration and operational decisions for clean energy. Moreover, we develop a computationally efficient methodology to solve the resulting large-scale problem by dividing it into two stages. Firstly, a set of time-aggregated scenarios representing the seasonal and daily variability in electricity price and renewable availability is utilized to obtain an optimal system design. Next, keeping the design decisions fixed, optimal hourly operational variables are computed for the original scenario set. This two-stage strategy strikes a balance between computational tractability and solution accuracy as we decouple the long-term design and the short-term operating decisions.

We demonstrate the framework through both statewide and nationwide case studies across the US. The results indicate that for a projected carbon tax above \$80 per ton and renewable energy prices below \$300 per kW, it is beneficial to integrate CO_2 capture with all the coal plants. Solar energy shows more promise than wind, with co-located solar PV farms selected for nearly one-third of the plants nationwide. Additionally, we observe a positive linear correlation of the optimal solar farm size with the nameplate capacity of the coal power plant, with the average size being around 25.8% of the nameplate capacity. Solar energy reduces the CO_2 capture cost by 8.9%. On the other hand, the CO_2 capture system cost-effectively counters renewable intermittency by avoiding an equivalent investment in battery storage amounting to 4.4 times the installed cost of the solar PV farm for storing the excess solar energy. Furthermore, the levelized cost of the integrated system is less than that of a new NGCC plant with achieved CO_2 emission reduction ranging between 87.5%-91%. To summarize, in a futuristic scenario with a price on emissions, coal plant operators should focus their investment efforts on the CO_2 capture-renewable energy hybrid system as compared to replacing the coal plant with a relatively cleaner NGCC unit. The integrated system reduces both the cost of carbon capture and the intermittency of renewables, facilitating the transition between the current fossil-based and future renewable-dominant power sectors.

Future works can study the integration with other fossil-based systems such as natural gas to reduce emissions. Although wind energy is not selected, more efficient wind turbines with higher capacity factors considering the effect of hub height can further facilitate wind energy integration. In addition, we have referred to previous works on the use of biomass energy for the integration in our literature review of Section 2. This work can also be extended to include such controllable renewable energy sources of biofuels and geothermal energy for studying the nationwide integration with coal plants.

Author contributions

Manali S. Zantye: Conceptualization, data curation, formal analysis, investigation, software, writing – original draft, writing – review & editing. Akhil Arora: Methodology, visualization. M. M. Faruque Hasan: Funding acquisition, resources, supervision, writing – review & editing.

Conflicts of interest

There are no conflicts to declare.

Acknowledgements

The authors gratefully acknowledge funding support from U.S. Department of Energy (Grant number DE-FE0031771). Part of this research was conducted with the advanced computing resources provided by Texas A&M High Performance Research Computing. The authors also thank Spyridon D. Tsolas (Texas A&M University) for helpful suggestions on structuring the manuscript.

Notes and references

1 U.S. Energy Information Administration, *Electricity Explained*, https://www.eia.gov/energyexplained/electricity/electricity-in-the-us.php, (accessed May 2020).

2 M. M. F. Hasan, R. C. Baliban, J. A. Elia and C. A. Floudas, *Ind. Eng. Chem. Res.*, 2012, **51**, 15642–15664.

3 M. M. F. Hasan, R. C. Baliban, J. A. Elia and C. A. Floudas, *Ind. Eng. Chem. Res.*, 2012, **51**, 15665–15682.

4 A. S. Bhown and B. C. Freeman, *Environ. Sci. Technol.*, 2011, **45**, 8624–8632.

5 M. M. F. Hasan, E. L. First, F. Boukouvala and C. A. Floudas, *Comput. Chem. Eng.*, 2015, **81**, 2–21.

6 M. M. F. Hasan, F. Boukouvala, E. L. First and C. A. Floudas, *Ind. Eng. Chem. Res.*, 2014, **53**, 7489–7506.

7 M. L. Godec, V. A. Kuuskraa and P. Dipietro, *Energy Fuels*, 2013, **27**, 4183–4189.

8 A. Arora, S. S. Iyer, I. Bajaj and M. M. F. Hasan, *Ind. Eng. Chem. Res.*, 2018, **57**, 14143–14161.

9 S. S. Iyer, I. Bajaj, P. Balasubramanian and M. M. F. Hasan, *Ind. Eng. Chem. Res.*, 2017, **56**, 8622–8648.

10 K. Roh, R. Frauzem, R. Gani and J. H. Lee, *Chem. Eng. Res. Des.*, 2016, **116**, 27–47.

11 E. S. Rubin, C. Chen and A. B. Rao, *Energy Policy*, 2007, **35**, 4444–4454.

12 J. Gibbins and H. Chalmers, *Energy Policy*, 2008, **36**, 4317–4322.

13 Global CCS Institute, *Global Status Report*, `https://www.globalccsinstitute.com/resources/global-status-report/`, (accessed May 2020).

14 M. S. Zantye, A. Arora and M. M. F. Hasan, *Comput. Chem. Eng.*, 2019, **130**, 106544.

15 N. Mac Dowell and N. Shah, *Energy Procedia*, 2014, **63**, 1525–1535.

16 S. M. Cohen, G. T. Rochelle and M. E. Webber, *Energy Procedia*, 2011, **4**, 2604–2611.

17 M. Zaman and J. H. Lee, *Comput. Chem. Eng.*, 2015, **75**, 14–27.

18 M. Pehl, A. Arvesen, F. Humpenöder, A. Popp, E. G. Hertwich and G. Luderer, *Nat. Energy*, 2017, **2**, 939–945.

19 M. Trifkovic, W. A. Marvin, P. Daoutidis and M. Sheikhzadeh, *AIChE J.*, 2014, **60**, 2546–2556.

20 G. Pleßmann, M. Erdmann, M. Hlusiak and C. Breyer, *Energy Procedia*, 2014, **46**, 22–31.

21 J. P. Barton and D. G. Infield, *IEEE Transactions on Energy Conversion*, 2004, **19**, 441–448.

22 K. Van den Bergh and E. Delarue, *Energy Convers. Manage.*, 2015, **97**, 70–77.

23 N. Kumar, P. Besuner, S. Lefton, D. Agan and D. Hilleman, *Power Plant Cycling Costs*, National Renewable Energy Lab. (NREL), Golden, CO (United States) technical report, 2012.

24 D. Aaron and C. Tsouris, *Sep. Sci. Technol.*, 2005, **40**, 321–348.

25 H. Chalmers and J. Gibbins, 29th IAEE International Conference, 2006.

26 S. M. Cohen, G. T. Rochelle and M. E. Webber, *Energy Procedia*, 2013, **37**, 2585–2594.

27 S. Ludig, M. Haller and N. Bauer, *Energy Procedia*, 2011, **4**, 2580–2587.

28 M. Nimtz and H.-J. Krautz, *Energy Procedia*, 2013, **40**, 294–303.

29 S. M. Cohen, G. T. Rochelle and M. E. Webber, Energy Sustainability, 2008, pp. 127–136.

30 U.S. Energy Information Administration, *Annual Energy Outlook 2020*, `https://www.eia.gov/outlooks/aeo/section_issue_renewables.phps`, (accessed May 2020).

31 F. Parvareh, M. Sharma, A. Qadir, D. Milani, R. Khalilpour, M. Chiesa and A. Abbas, *Renewable Sustainable Energy Rev.*, 2014, **38**, 1029–1044.

32 S. Cohen and G. Rochelle, ASME 4th International Conference on Energy Sustainability, Phoenix, 2010.

33 M. Mokhtar, M. T. Ali, R. Khalilpour, A. Abbas, N. Shah, A. Al Hajaj, P. Armstrong, M. Chiesa and S. Sgouridis, *Appl. Energy*, 2012, **92**, 668–676.

34 H. Li, J. Yan and P. E. Campana, *Int. J. Greenhouse Gas Control*, 2012, **9**, 272–280.

35 A. Qadir, M. Sharma, F. Parvareh, R. Khalilpour and A. Abbas, *Energy Convers. Manage.*, 2015, **97**, 7–19.

36 Y. Zhao, H. Hong, X. Zhang and H. Jin, *Sol. Energy*, 2012, **86**, 3196–3204.

37 C. A. Kang, A. R. Brandt and L. J. Durlofsky, *Energy*, 2011, **36**, 6806–6820.

38 R. Bandyopadhyay and D. Patiño-Echeverri, *Renewable Energy*, 2016, **85**, 704–713.

39 A. Phadke, C. Goldman, D. Larson, T. Carr, L. Rath, P. Balash and W. Yih-Huei, *Advanced Coal Wind Hybrid: Economic Analysis*, Lawrence Berkeley National Lab.(LBNL), Berkeley, CA (United States) technical report, 2008.

40 R. Carapellucci, L. Giordano and M. Vaccarelli, *Energy Procedia*, 2015, **82**, 350–357.

41 Z. Khorshidi, M. T. Ho and D. E. Wiley, *Int. J. Greenhouse Gas Control*, 2015, **32**, 24–36.

42 S. Gouse, D. Gray and G. Tomlinson, *Energy Convers. Manage.*, 1993, **34**, 1023–1030.

43 M. S. Jassim and G. T. Rochelle, *Ind. Eng. Chem. Res.*, 2006, **45**, 2465–2472.

44 E. Esposito, L. Dellamuzia, U. Moretti, A. Fuoco, L. Giorno and J. C. Jansen, *Energy Environ. Sci.*, 2019, **12**, 281–289.

45 B. Metz, O. Davidson, H. De Coninck *et al.*, *Carbon Dioxide Capture and Storage: Special Report of the Intergovernmental Panel on Climate Change*, Cambridge University Press, 2005.

46 U.S. Environmental Protection Agency (EPA), *Greenhouse Gas Reporting Program (GHGRP)*, `https://www.epa.gov/ghgreporting`, (accessed March 2021).

47 M. Zachar, M. Trifkovic and P. Daoutidis, *Comput. Chem. Eng.*, 2015, **81**, 364–375.

48 M. J. Palys and P. Daoutidis, *Comput. Chem. Eng.*, 2020, 106785.

49 Q. Chen, C. Kang, Q. Xia and D. S. Kirschen, *IEEE Transactions on Power Systems*, 2012, **27**, 1602–1609.

50 W. W. Tso, C. D. Demirhan, C. F. Heuberger, J. B. Powell and E. N. Pistikopoulos, *Appl. Energy*, 2020, **270**, 115190.

51 C. L. Lara, D. S. Mallapragada, D. J. Papageorgiou,

A. Venkatesh and I. E. Grossmann, *European Journal of Operational Research*, 2018, **271**, 1037–1054.

52 P. Gabrielli, M. Gazzani, E. Martelli and M. Mazzotti, *Appl. Energy*, 2018, **219**, 408–424.

53 M. Zatti, M. Gabba, M. Freschini, M. Rossi, A. Gambarotta, M. Morini and E. Martelli, *Energy*, 2019, **181**, 1051–1063.

54 C. F. Heuberger, I. Staffell, N. Shah and N. Mac Dowell, *Comput. Chem. Eng.*, 2017, **107**, 247–256.

55 S. Pineda and J. M. Morales, *IEEE Transactions on Power Systems*, 2018, **33**, 7162–7170.

56 J. Dupačová, N. Gröwe-Kuska and W. Römisch, *Mathematical Programming*, 2003, **95**, 493–511.

57 GAMS, *The General Algebraic Modeling System: User Guide*, https://www.gams.com/33/docs/UG_MAIN.html, (accessed March 2021).

58 National Renewable Energy Laboratory (NREL), *National Solar Radiation Database*, https://nsrdb.nrel.gov/, (accessed May 2020).

59 H. Heitsch and W. Römisch, *Operations Research Letters*, 2007, **35**, 731–738.

60 *Electric Reliability Council of Texas*, www.ercot.com, (accessed May 2020).

61 *Southwest Power Pool*, spp.org, (accessed May 2020).

62 U.S. Environmental Protection Agency (EPA), *Emissions & Generation Resource Integrated Database (eGRID)*, https://www.epa.gov/egrid, (accessed May 2020).

63 U.S. Energy Information Administration, *Today in Energy*, https://www.eia.gov/todayinenergy/detail.php?id=44636#, (accessed December 2020).

64 Federal Energy Regulatory Commission, *Electric Power Markets*, cms.ferc.gov/industries-data/market-assessments/overview/electric-power-markets, (accessed May 2020).

65 N. V. Sahinidis, *Journal of Global Optimization*, 1996, **8**, 201–205.

66 The Center on Global Energy Policy at Columbia University SIPA, *What You Need to Know About a Federal Carbon Tax in the United States*, https://www.energypolicy.columbia.edu, (accessed March 2021).

67 Harvard Law School: Environmental & Energy Law Program, *President-Elect Biden Supports a "Carbon Enforcement Mechanism" – Could that Mean a Price on Carbon?*, https://eelp.law.harvard.edu/2020/11, (accessed March 2021).

68 U.S. Department of Energy, *Internal Revenue Code Tax Fact Sheet*, https://www.energy.gov/sites/prod/files/2019/10/f67/Internal%20Revenue%20Code%20Tax%20Fact%20Sheet.pdf, (accessed March 2021).

69 C. Murphy, Y. Sun, W. J. Cole, G. J. Maclaurin, M. S. Mehos and C. S. Turchi, *The Potential Role of Concentrating Solar Power within the Context of DOE's 2030 Solar Cost Targets*, National Renewable Energy Lab. (NREL), Golden, CO (United States) technical report, 2019.

70 U.S. Energy Information Administration, *Levelized Cost and Levelized Avoided Cost of New Generation Resources in the Annual Energy Outlook 2020*, https://www.eia.gov/outlooks/aeo/pdf/electricity_generation.pdf, (accessed October 2020).

71 F. Wang, S. Deng, J. Zhao, J. Zhao, G. Yang and J. Yan, *Energy Convers. Manage.*, 2017, **148**, 569–582.

72 J. Oexmann and A. Kather, *Energy Procedia*, 2009, **1**, 799–806.

73 U.S. Energy Information Administration, *How much carbon dioxide is produced per kilowatthour of U.S. electricity generation?*, https://www.eia.gov/tools/faqs/faq.php?id=74&t=11, (accessed March 2021).

74 D. Schlissel and D. Wamsted, *Holy Grail of Carbon Capture Continues to Elude Coal Industry*, Institute for Energy Economics and Financial Analysis (IEEFA) technical report, 2018.

75 K. Mongird, V. V. Viswanathan, P. J. Balducci, M. J. E. Alam, V. Fotedar, V. S. Koritarov and B. Hadjerioua, *Energy Storage Technology and Cost Characterization Report*, Pacific Northwest National Lab. (PNNL), Richland, WA (United States) technical report, 2019.

76 U.S. Energy Information Administration, *State Profile and Energy Estimates: Texas*, https://www.eia.gov/state/analysis.php?sid=TX, (accessed December 2020).

77 S&P Global, *Market Intelligence*, https://www.spglobal.com/marketintelligence/en/, (accessed May 2020).

78 Inside Climate News, *CPS Energy to Shut Coal-Fired Plant in Texas, Turn to Renewables*, https://insideclimatenews.org/news/21062011, (accessed March 2021).

79 Sierra Club, *UPDATE: Gibbons Creek Coal Plant Gets Approval to Shut Down Indefinitely, Electric Generators Get More Money*, https://www.sierraclub.org/texas/blog, (accessed March 2021).